

# ICESat-2 Onboard Flight Receiver Algorithms: On-orbit Parameter Updates the Impact on Science Driven Observations

Lori A. Magruder<sup>1</sup>, Ann R Reese<sup>2</sup>, Aimée Gibbons<sup>3</sup>, James T. Dietrich<sup>4</sup>, and Thomas A Neumann<sup>5</sup>

<sup>1</sup>University of Texas at Austin

<sup>2</sup>KBR @NASA/GSFC

<sup>3</sup>KBR

<sup>4</sup>Unknown

<sup>5</sup>NASA Goddard Space Flight Center

January 23, 2024

## Abstract

The ICESat-2 (Ice, Cloud and Land Elevation Satellite-2) photon-counting laser altimeter technology required the design and development of very sophisticated onboard algorithms to collect, store and downlink the observations. These algorithms utilize both software and hardware solutions for meeting data volume requirements and optimizing the science achievable via ICESat-2 measurements. Careful planning and dedicated development were accomplished during the pre-launch phase of the mission in preparation for the 2018 launch. Once on-orbit all of the systems and subsystems were evaluated for performance, including the receiver algorithms, to ensure compliance with mission standards and satisfy the mission science objectives. As the mission has progressed and the instrument performance and data volumes were better understood, there have been several opportunities to enhance ICESat-2's contributions to earth observation science initiated by NASA and the ICESat-2 science community. We highlight multiple updates to the flight receiver algorithms, the onboard software for signal processing, that have extended ICESat-2's data capabilities and allowed for advanced science applications beyond the original mission objectives.

1 **ICESat-2 Onboard Flight Receiver Algorithms: On-orbit Parameter Updates**  
2 **the Impact on Science Driven Observations**

3  
4 Lori Magruder<sup>1</sup>, Ann Rackley Reese<sup>2,3</sup>, Aimée Gibbons<sup>2,3</sup> James Dietrich<sup>1</sup> and Tom Neumann<sup>3</sup>

5 <sup>1</sup>Center for Space Research, University of Texas at Austin, Austin, TX.

6 <sup>2</sup>KBR, Greenbelt, MD

7 <sup>3</sup>NASA Goddard Space Flight Center, Greenbelt, MD

8  
9 Corresponding author: Lori Magruder<sup>†</sup> ([lori.magruder@austin.utexas.edu](mailto:lori.magruder@austin.utexas.edu))

10  
11 Key Points:

- 12 ● Since the 2018 ICESat-2 launch multiple updates have been made to the satellite's  
13 onboard flight receiver algorithm parameters to improve access and utility of the data for  
14 a multi-disciplinary science community
- 15 ● The adjustments have been primarily in the in the vertical telemetry window settings and  
16 have facilitated enhanced observations of blowing snow and increased detection  
17 opportunities of bathymetry in nearshore environments
- 18 ● The parameter changes have been made to mitigate data losses in certain situations and  
19 to advance science applications outside of the primary science objectives of the ICESat-2  
20 mission.

21

22 **Abstract**

23 The ICESat-2 (Ice, Cloud and Land Elevation Satellite-2) photon-counting laser altimeter  
24 technology required the design and development of very sophisticated onboard algorithms to  
25 collect, store and downlink the observations. These algorithms utilize both software and  
26 hardware solutions for meeting data volume requirements and optimizing the science achievable  
27 via ICESat-2 measurements. Careful planning and dedicated development were accomplished  
28 during the pre-launch phase of the mission in preparation for the 2018 launch. Once on-orbit all  
29 of the systems and subsystems were evaluated for performance, including the receiver  
30 algorithms, to ensure compliance with mission standards and satisfy the mission science  
31 objectives. As the mission has progressed and the instrument performance and data volumes  
32 were better understood, there have been several opportunities to enhance ICESat-2's  
33 contributions to earth observation science initiated by NASA and the ICESat-2 science  
34 community. We highlight multiple updates to the flight receiver algorithms, the onboard  
35 software for signal processing, that have extended ICESat-2's data capabilities and allowed for  
36 advanced science applications beyond the original mission objectives.

37 **Plain Language Summary**

38 NASA launched its second Earth observing laser altimeter in 2018 with mission objectives of  
39 collecting observations in support of Earth science as a window into climate change impacts on  
40 our planet. Pre-launch studies focused on specific instrument settings and on-board data  
41 processing to support the mission objectives without violating data volume constraints. Once the  
42 instrument was on-orbit and operational, evaluation of the algorithms for success in signal  
43 detection, signal finding, and signal telemetry was undertaken. In response to the evaluation,  
44 updates have been made to optimize the data provided by the mission.

45 **1. Introduction**

46 The Ice, Cloud and land Elevation Satellite-2 (ICESat-2) has been providing global height  
47 measurements to the scientific community since 2018. ICESat-2 has similar scientific objectives  
48 as its predecessor mission, ICESat (Schutz et al. 2005), with a focus on using satellite laser  
49 altimetry to support climate variable monitoring as a window to understanding Earth's response  
50 to a changing climate. The primary instrument onboard ICESat-2 is the Advanced Topographic  
51 Laser Altimetry System (ATLAS) and is one of the most technically advanced space-borne lidar  
52 for Earth Science to date (Martino et al. 2019). ATLAS is a photon-counting lidar, sensitive to  
53 single photon reflections from the surface of the Earth. The photon-counting technology  
54 facilitates the use of lower laser energy, creating a scenario where multiple beams and higher  
55 laser repetition rates allow for greater spatial coverage and higher spatial resolution, both of  
56 which were implemented improvements based on operational realizations identified by the  
57 predecessor mission (ICESat) (Markus et al. 2017; Magruder et al. 2021). The high repetition rate  
58 (10kHz) provides higher along-track spatial resolution and the capability to capture fine scale  
59 features on the surface in time and space to meet requirements associated with dynamic  
60 processes in our Polar Regions. The multiple beam configuration allows for the discrimination  
61 between surface slope and true elevation change in the case of repeat measurements (Smith et al.  
62 2020). ICESat-2 mission requirements are described by Markus et al. (2017) and successful  
63 completion of the requirements is summarized in Magruder et al., 2024 (Magruder et al. 2024).  
64 The large data volume associated with a photon counting lidar was anticipated and the approach  
65 to onboard data management and signal processing techniques had to be altered from previous  
66 missions. It was understood and expected that ATLAS would exceed the normal X-band radio  
67 downlink capabilities and could require additional downlink station contacts (McGarry et al.

68 2021). The ICESat-2 Project Science Office (PSO) made the decision early in the pre-launch  
69 mission phase to focus on reducing the data volume onboard via processing algorithms and then  
70 determine if there was a need for more ground station access. The onboard algorithms that  
71 comprise the flight software (FSW) were designed to provide a sophisticated means for signal  
72 finding and data reduction. These functions are performed through inventive use of onboard  
73 signal processing, databases, and telemetry window selection across the diversity of global  
74 environments and surface types (Leigh et al. 2015; McGarry et al. 2021). Each component of the  
75 comprehensive FSW was created around the idea of having flexible parameterization to  
76 accommodate on-orbit adjustments, changes, and updates as the mission matured and discoveries  
77 of future, unanticipated needs are identified through the prime mission lifetime and into the  
78 extended mission timeline.

79 The majority of the data volume acquired by ATLAS during each orbit and between downlink  
80 opportunities occurs during daylight hours. This accumulation is due to the nature of photon-  
81 counting systems, as ATLAS is susceptible to solar background noise entering the system at the  
82 same wavelength to the ATLAS laser (532 nm). During the day the ambient background noise  
83 can exceed 10 MHz, which creates the need for noise mitigation processing in order to not  
84 violate the telemetry constraints associated with downlink bandwidth limitations. Whether noise  
85 or signal, ATLAS detects and records the time of arrival for every received photon creating a  
86 disparity among detection types based on an extremely low signal to noise ratio (Anthony J.  
87 Martino et al. 2019). These challenges created a need for optimizing onboard techniques for  
88 ensuring capture of the surface signal without possible data losses associated with overloading  
89 downlink opportunities.

90 The overarching requirements for the onboard receiver algorithm FSW are: 1) Keep the average

91 daily science telemetry data volume below 577.4 Gb/day, 2) Use the real time position and  
92 attitude solutions to guide the surface signal finding within 2 km horizontally and 250 m  
93 vertically for off-nadir angles between  $0^\circ$  and  $\pm 5^\circ$  (with capabilities up to  $\pm 10^\circ$  off-nadir pointing  
94 after July 20, 2023), and 3) Select/find surface signal at least 90% of the time in regions of  
95 optically thin cloud cover, but not constrained by surface reflectivity, topography or solar  
96 elevation angle.

97 The utility of the receiver algorithms is to meet the volume constraints while capturing a  
98 complete and accurate altimetry signal of surface elevations. This is accomplished through  
99 several complementary functions that involve signal processing and functions that use a set of  
100 onboard databases of Earth elevations and topographic relief to inform where to look for true  
101 surface signal. Once the approximate surface is determined, the algorithm can align an  
102 appropriate telemetry window to ensure appropriate signal retention and successful data  
103 downlink. Comprehensive descriptions of the onboard receiver algorithm operations and  
104 capabilities are well described in the previous publications (Leigh et al. 2015; McGarry et al.  
105 2021) but will be mentioned in the subsequent sections for completion.

106 This article provides an overview of changes that have been made to the ICESat-2 FSW and  
107 receiver algorithms since launch. The FSW updates have been made to enhance ICESat-2's  
108 usefulness across a wide range of earth observation topics, including measurements of blowing  
109 snow and coastal bathymetry. We provide an overview of FSW and then discuss each update and  
110 the impact on ICESat-2 data products and the applications to earth observation science.

## 111 **1.1 Signal processing**

112 The Photon Counting Electronics (PCE) cards operate on each pair of strong and weak  
113 beams. The PCEs record the transmit and receive times of photons for each ATLAS pulse. Using

114 the transmit and receive times the time of flight (TOF) can be calculated and used to generate  
115 coarse range values that are then used to produce histograms of photon arrival times. The  
116 histograms are aggregates of 200 consecutive laser shots, corresponding to an along-track  
117 distance of 140 m (or 0.02 s) (McGarry et al. 2021). The flight software uses the histograms to  
118 perform initial signal and background rate estimates to inform data downlink criteria.

119 For two of the three strong beams a portion of the laser energy is redirected back to the  
120 receiver channel instead of being transmitted to the surface. This laser pickoff, called the TEP  
121 (Transmitted Echo Path), is fixed relative to the time of laser fire from which it was generated,  
122 with the primary pulse peak time-of-flight around 18-19 ns. The TEP is only recorded when it  
123 falls within the range window (RW) for a given laser fire but allows the instrument to record the  
124 shape of the outgoing laser pulse, providing a means to monitor the health and data quality of  
125 ATLAS. It also facilitates the identification of deteriorated conditions, such as transmit/receive  
126 pulse slips and fine count swaps. The most recent TEP photons meeting certain quality criteria  
127 are carried onto the ATL03 data product as ancillary information (Neumann et al. 2019).

## 128 **1.2 Databases and Telemetry window selection**

129 The next signal finding step is performed on the detected photons that exist within the  
130 determined range window through a combination of software and hardware approaches. The  
131 primary function of this step is to determine the appropriately sized vertical telemetry band that  
132 will encompass the surface photon reflections and limit excess data volume caused by noise  
133 photons and be telemetered down to ground stations for further processing. The telemetry band is  
134 defined as the vertical extent for which detected photons (signal and noise) are downlinked. The  
135 RW is ultimately determined by an onboard digital elevation model (DEM) that contains the  
136 minimum and maximum elevations globally. These elevation grids are indexed by latitude and

137 longitude and meet the requirement of 150 m ( $3\sigma$ ) accuracy (McGarry et al. 2021). The RW is  
138 constrained to a vertical maximum of 6 km that includes a  $\pm 250$  m height margin. To meet this  
139 requirement the onboard DEM is actually comprised of a tertiary grid system of varying  
140 resolutions ( $1^\circ \times 1^\circ$ ,  $0.25^\circ \times 0.25^\circ$ ,  $0.05^\circ \times 0.05^\circ$ ) to maintain that the relief (vertical distance  
141 between maximum and minimum elevation at a given geographical location) does not exceed  
142 5500 m. The baseline for where the expected surface elevation can be found within the vertical  
143 window is derived from the void-filled SRTM (Shuttle Radar Topography Mission) product  
144 released by the CGIAR-CSI (Consortium for Spatial Information; SRTM-CGIAR (Jarvis et al.  
145 2008)) for the mid-latitudes and other available DEMs outside of the SRTM latitudinal reach  
146 (e.g. Greenland Ice Mapping Project (GIMP), Bedmap2, Global Multi-resolution Terrain  
147 elevation Data (GMTED), and the Canadian Digital elevation Database (CDED)). The  
148 EGM2008 geoid is used to estimate the ocean surface elevations (Leigh et al. 2015).

149         The global relief database is the second type of database onboard ICESat-2. This DRM  
150 (digital relief model) establishes the elevation range surrounding the identified ground signal that  
151 is incorporated into the telemetry band calculation, along with padding and offset parameters.  
152 The DRM is assembled at a resolution of  $0.25^\circ \times 0.25^\circ$ , and contains the maximum relief values  
153 across two length scales (140 m and 700 m) (Leigh et al. 2015). The DRM relief values overlay  
154 the signal bin representing the perceived or apparent ground, helping ascertain the number of  
155 adjacent bins to incorporate into the downlink telemetry, aside from the signal bin itself. Failing  
156 to include the DRM relief values could result in the omission of ground and canopy signals in  
157 rugged and/or vegetated regions from the downlinked data. The DEM and DRM databases were  
158 enhanced by incorporating global vegetation heights obtained from Simard et al. (2011) (Simard  
159 et al. 2011).

160 The third type of database onboard ICESat-2 is the Surface Reference Mask (SRM) and, like the  
161 DRM, is at a resolution of  $0.25^\circ \times 0.25^\circ$ . The SRM classifies the surface type, as a means to  
162 define values of vertical (elevation) padding required for the telemetry window. This is used to  
163 accommodate (and mitigate) the uncertainties in the relief estimates and geolocation knowledge.  
164 The SRM also indicates if there is vegetation, and if there is coastline for each tile. The four  
165 possible surface types are land ice, sea ice, land, and ocean with precedence given in that order  
166 for mask cells that cover multiple surface types (McGarry et al. 2021).

## 167 **2. Materials and Methods**

168 As part of the ATLAS FSW, the receiver algorithms use several adjustable parameter  
169 files that allow modifications to the signal processing elements of the software to be updated  
170 without having to modify or update the underlying code of the FSW and receiver algorithms.  
171 Many of the parameters are determined as a function of either surface type, spot type (i.e. beam  
172 energy), or day or night conditions allowing for fine-tuned and discipline specific adjustments.  
173 The values are specified in a set of three parameter files. Each of the three onboard PCE  
174 detectors have an independent set of files, however all three PCE parameter files are  
175 synchronized to the same update version. The receiver algorithm parameter file types and their  
176 parameters that are frequently updated are described in the following sections.

### 177 **2.1 “Knobs” files (nominal and alternate parameters)**

178 The Knobs files contain parameters that allow control over the data volume by selecting  
179 content in the telemetry downlink and the conditions associated with when to telemeter data.  
180 Each PCE has a nominal Knobs file and an Alternate Knobs file. The nominal Knobs files are  
181 optimized for the main science objectives and keeping the data volume within the daily limit.  
182 The Alternate Knobs are used for those situations where the satellite is performing maneuvers

183 associated with ocean scans, round-the-world scans (Luthcke et al. 2021), and targets of  
184 opportunity (Magruder et al. 2021). The Alternate Knobs files create a configuration that  
185 continuously telemeters data regardless of surface type, time of day, or signal type. Only one  
186 Knobs file type is in use at a time for each PCE.

187         The telemetry “Knobs” parameters control what data to telemeter, or the content of the  
188 downlink. There are knobs for the numerous possible signal conditions, categorized by surface  
189 type, day or night acquisition, and spot strength (strong or weak). The No-signal Timer  
190 parameters count the number of consecutive Major Frames (nominally 200 laser pulses) to  
191 telemeter when no signal is identified by the receiver algorithms. There are two timer states,  
192 timer1 and timer2. The receiver algorithms enter the timer1 state when no signal is found for a  
193 major frame and the knobs are configured to still telemeter data. Timer1 currently varies from 10  
194 to 50 major frames, depending on the surface type. Timer2 begins when timer1 has expired and  
195 currently varies from 100 major frames to no expiration, depending on the surface type. The  
196 timer2 state generally consists of vertically larger telemetry bands. If timer2 expires then no data  
197 is selected to telemeter until signal is found again.

## 198         **2.2 PPR (Position, Pointing, and Range parameters)**

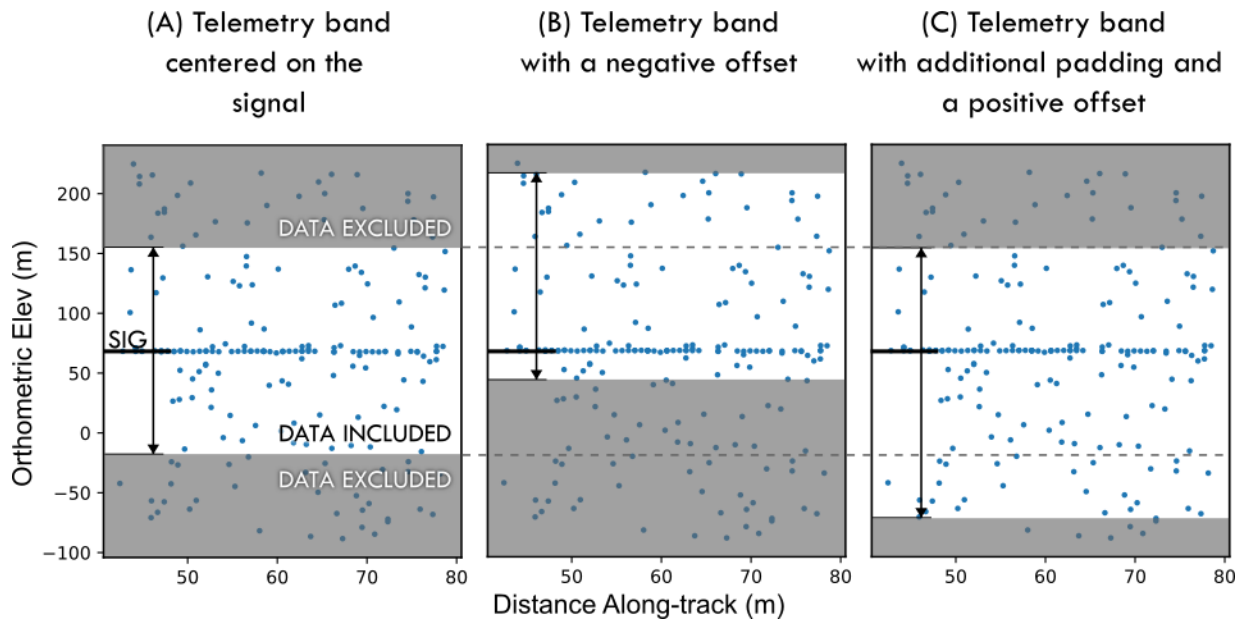
199         The PPR files contain parameters associated with calculating each spot location on Earth  
200 and setting the Range Window (search area to look for signal). The Range Window Minimum  
201 Width parameters define the minimum allowed vertical width of the range window. It can be set  
202 separately for each surface type, day or night, and strong or weak spot.

## 203         **2.3 ST (Signal and Telemetry parameters)**

204         The ST files contain parameters used in signal processing and calculating the vertical  
205 width of the telemetry bands. The telemetry band padding parameters define the amount of

206 margin to add in the calculation of the telemetry band width. The padding value is doubled and  
207 added to the scaled relief to account for uncertainties in the relief value. The relief comes from  
208 the onboard DRM and the scale factor is a parameter in the ST file. The padding parameters are a  
209 function of surface type, spot type and relief value. There are four ranges of relief (R) values ( $R$   
210  $\leq 189$  m,  $189$  m  $< R \leq 567$  m,  $567$  m  $< R \leq 1323$  m,  $1323$  m  $< R$ ) which specify the interval of  
211 padding to use. Generally, the padding values increase with each interval, except for ocean  
212 surface types.

213         The telemetry band offset and padding parameters define the position and shape of the  
214 telemetry band in vertical space (Figure 1). Offsets can be applied to shift the telemetry band up  
215 or down, a positive offset shifts the telemetry band down in vertical space and a negative offset  
216 shifts the telemetry band up in vertical space. An offset of 0 centers the telemetry band around  
217 the signal location. Padding is applied based on the onboard DRM values and increases the  
218 overall height of the telemetry band (symmetrically around the signal position). Offset and  
219 padding can be applied independently or in concert with each other to achieve the necessary  
220 telemetry band.



221  
 222 Figure 1. Diagram illustrating the different adjustments that are available when defining the  
 223 telemetry window. 200-photon returns are illustrated in each plot and data that would be  
 224 excluded (not downlinked) are shown in the gray boxes. (a) shows a normally centered telemetry  
 225 window around a signal (ground surface) at ~60 m elevation, (b) the window with the same  
 226 height as (a) with a negative offset applied to capture more data above the signal surface, and (c)  
 227 increased padding applied and a positive offset to increase the amount of data below the signal  
 228 surface while maintaining the height of the window limit above the signal.  
 229

### 230 3. Summary of on-orbit changes

231 Parameter file Versions 01 through 05 cover the work done in pre-launch simulated testing,  
 232 Integration and Testing (I&T), and observatory testing. ICESat-2 launched on 15 September  
 233 2018 operating on Version 06 parameter files (McGarry et al., 2020). Since launch, there have  
 234 been five version updates to the operational parameter files. As of this writing, ICESat-2 is  
 235 operating on Version 14. There are several file versions tested on-orbit or only in simulated  
 236 testing that were never made operational (07, 09 and 12). Table 1 has a summary of the testing  
 237 and operational timelines for each operational version since launch.

238  
 239

240

241 Table 1. Parameter file version test dates, test durations and operational start dates. Versions 07  
 242 and 09 were tested on-orbit, but never made operational. Version 12 was not tested on-orbit and is  
 243 therefore excluded from the table. \*Due to resetting of PCE1 and PCE3, there are gaps in usage of  
 244 v14: 29 Dec 22 - 6 Feb 23 for PCE1 and 2 Feb 23 - 6 Feb 23 for PCE3.

Version	Test Start Date	Test Duration (approx.)	Date Operational	Description
06	--	--	15 Sept 2018	Launch version
07	4 Apr 2019	4 hours	--	Data enhancements (TEP crossing signal) Corrected range window settings
08	9 May 2019	5 hours	3 Sept 2019	Data enhancements (TEP crossing signal, ocean, blowing snow) Corrected range window settings
09	25 Oct 2019	2 days	--	Data enhancements (lake bathymetry)
10	17 Nov 2020	2 weeks	27 Jan 2021	Data enhancements (ocean bathymetry)
11	16 Feb 2021	3.5 hours	12 Mar 2021	Error mitigation related to range windows
13	18 May 2021	5 hours	1 June 2021	Data enhancements (weak spot ocean)
14	1 Nov 2022	30 days	1 Dec 2022 *	Data enhancements (coastline bathymetry)

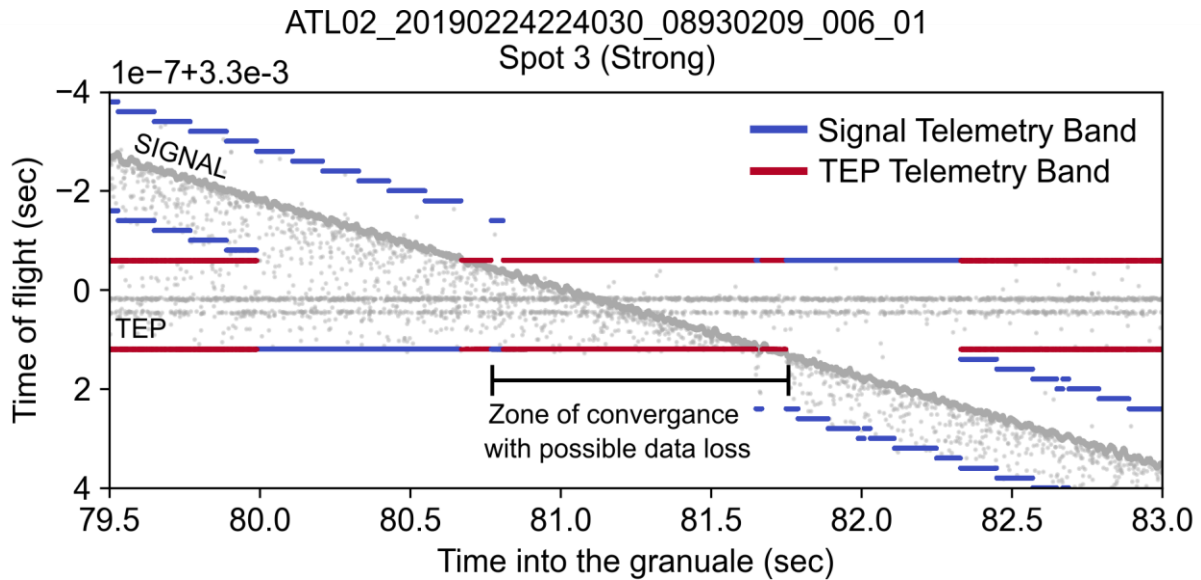
245

### 246 **3.1 Version 08: TEP Signal Crossing, Ocean and Blowing Snow Band Widths**

247 The first operational version revision of the parameter files is Version 08 was tested on  
 248 orbit in May 2019 and made operational on 3 September 2019. This version includes changes to  
 249 the Knobs, PPR, and ST files. Version 08 updates incorporated three major changes: 1)  
 250 mitigating the loss of data when the Transmitter Echo Path (TEP) is close to surface, which  
 251 reduced the range window widths for non-TEP photons to the nominal value 2) increasing  
 252 telemetry band widths to capture blowing snow and 3) increased telemetry band widths more  
 253 area around the open ocean surfaces.

254 The first Knobs file update mitigates data losses when the TEP is close to an ocean or sea  
 255 ice surface, shown in Figure 2 for the ocean. The nominal parameter settings tell the receiver

256 algorithms to ignore the area around the TEP (~27 meter vertical window) when searching for  
257 surface signal to avoid selecting the TEP as signal. This logic combined with the TEP  
258 approaching a flat surface can result in multiple Major Frames of missed surface data. In order to  
259 preserve signal data when the TEP intersects with the surface return, the Knobs parameters for  
260 the strong spots over ocean are turned on when no signal is found via the standard  
261 histogramming approach. The no-signal timer1 for both ocean and sea ice was reduced from 25  
262 Major Frames to 10 Major Frames and the no-signal timer2 is set to continuously telemeter data.  
263 By switching to the no-signal timer2 state sooner, the telemetry bands are set to the width of the  
264 range window ensuring both the TEP and surface are captured until there is sufficient distance  
265 between the TEP and surface, on the order of approximately 20 m for ocean and sea ice. This  
266 approximation allows for the established histogram bin size of ~12 m for ocean or sea ice surface  
267 signal and ~27 m for the TEP. Assuming the surface signal is in the middle of the bin (6 m on  
268 each side) and the TEP is in the middle of the bin (14 m on each side) the result is the 20 m  
269 estimate but in general the range is ~14 m to ~24 m.  
270



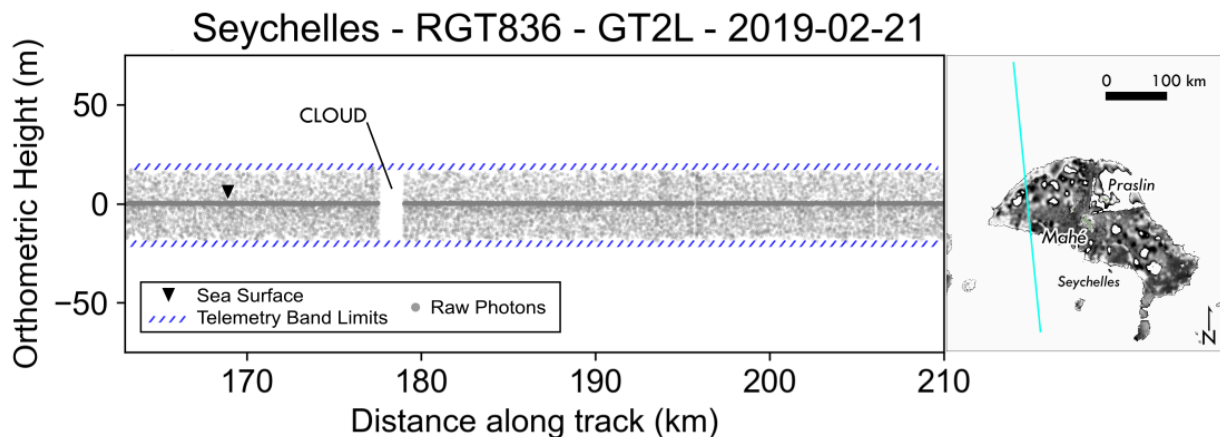
271  
 272 Figure 2. Due to the logic of handling the TEP within the receiver algorithms, some Major  
 273 Frames clip the ocean surface as it converges with the TEP. At about 80.75 seconds and 81.75  
 274 seconds the ocean surface is right at the bounds of the telemetry band, which is centered about  
 275 and sized for the TEP.  
 276

277         The second Knobs file update resolves an inconsistency between the receiver algorithms  
 278 and the flight software by removing the 140 m scale relief data (DRM-140) as an option for the  
 279 no-signal telemetry band relief in the timer2 state. The correct options for the no-signal telemetry  
 280 band relief in the timer2 state are the DEM (the nominal setting) or the 700 m scale relief data  
 281 (DRM-700). Note that both changes are replicated in the Alternate Knobs files where applicable.  
 282 The launch version of the PPR parameter files force the range windows for strong spots over sea  
 283 ice and land ice at night to a minimum of 5 km to capture the TEP. Because the TEP is only  
 284 present in two of the six spots (#1 and #3), the 5 km range window width minimum setting for  
 285 the remaining strong spot (#5) was reduced to the nominal minimum value of 500 meters.  
 286 At the request of the ICESat-2 Science Team, the telemetry band widths for the ocean, land ice  
 287 and sea ice surface types were increased in the ST files. The ocean telemetry bands gain 20  
 288 meters in total by increasing the telemetry band padding parameter by 10 meters, resulting in

289 ocean telemetry bands of 48 m in vertical height ( $\pm 24$  m above and below the signal). The land  
290 ice and sea ice telemetry bands are extended upwards by 30 meters to better capture blowing  
291 snow. This is accomplished by increasing the telemetry band padding by 15 meters and applying  
292 a -15-meter offset.

### 293 3.2 Version 10: Ocean Bathymetry

294 Several ICESat-2 Science Team members have focused on understanding the bathymetric  
295 capabilities of ATLAS once on-orbit and it was discovered that there were areas of clipped  
296 bathymetry data in open ocean tracks. This was due to the variable nature of the telemetry band  
297 limits along the coastlines and in open ocean. Figure 3 shows an example in the Indian Ocean in  
298 the Seychelles where shallow reef bathymetry has been excluded by the telemetry band size  
299 constraints. Bathymetric returns generally reach to 30 m below the water surface, and  
300 occasionally to 50 m (Parrish et al. 2019).



301  
302 Figure 3. An open ocean ground track showing the pre-Version 10 update telemetry band limits  
303 in the Seychelles. The shallow reef system to the west of Mahe island has known bathymetry that  
304 is less than 50 m deep and should be retrievable by ICESat-2, but has been excluded from the  
305 data because of the telemetry band limits (used with permission from Dietrich et al., 2023).  
306

307 Previously, the ocean telemetry bands spanned 48 m centered on the predicted surface,  
308 meaning they only reached 24 m below the surface. To reduce ocean bathymetry clipping, the

309 strong beam ocean telemetry bands were extended to reach at least 54 m below the surface by  
310 adjusting the padding and offset parameters. The vertical padding was increased by 15 m to 39 m  
311 and a vertical offset of +15 m is applied. The new padding and offset values extend the telemetry  
312 band deeper below the predicted surface while leaving the above surface limit unchanged.  
313 Utilizing the offset parameter allows for a smaller increase to the padding to extend to the  
314 desired depth, reducing the potential increase to the data volume. The padding and offset  
315 parameter changes are applied to the three strong spots and affect all ocean telemetry bands, not  
316 just areas with possible bathymetry (Dietrich et al. 2023).

317         Because the nominal parameters at the time of the version 10 update were set to not  
318 downlink weak spots data over oceans, no changes were made to the weak spot parameters  
319 because the weak spots are less likely to produce bathymetry (citations for less bathy in weak  
320 spots). A future (V13) update added the ability to telemeter weak spot ocean data., however the  
321 Version 10 changes for bathymetry capture are not applied as. The Alternate Knobs in version 10  
322 allowed for weak spot data to be downlinked, but the weak spot ocean telemetry bands did not  
323 have the increased padding and offset settings used in the strong spots. For more details on  
324 receiver algorithm updates related to bathymetric data acquisition (Versions 10 and 14), see  
325 Dietrich et al. (2023).

### 326         **3.3 Version 11: Range Window Error Mitigation**

327         In late 2020, an issue was discovered in which certain alignments of a strong/weak pair of  
328 range windows can trigger an error in the Data Flow Controller (DFC) logic, called a  
329 transmit/receive pulse (Tx/Rx) slip. When a Tx/Rx slip occurs, the ATL02 product generation  
330 code detects and corrects the error as detailed in Martino et al. ((Martino et al. 2019), Section  
331 2.5.7.3). In rare cases the error cannot be fixed with the current software, and the granule fails

332 before an ATL03 product file is generated. The error can be triggered at any time, but most  
333 frequently occurs when the range windows are forced “open”. In parameter file Versions 08  
334 through 10, the range windows for spots 1 and 3 are set to a minimum width of 5000 m to  
335 increase the frequency that the TEP can be captured. By forcing the range window for these  
336 strong spots to be much wider than they may be otherwise, the starts of the strong and weak spot  
337 range windows are more frequently farther apart, conditions which increase the likelihood of  
338 triggering the error. This is further supported by the decreased frequency of the error for PCE3,  
339 which does not include TEP, and whose strong-weak pair always have equivalent range window  
340 width minimums.

341 To mitigate the issue, the PPR files are updated to no longer force the range windows for  
342 spots 1 and 3 over land ice and sea ice at night to a minimum of 5000 m. The range window  
343 width minimums are updated to the nominal value of 500 m. This change does not fix the DFC  
344 logic error, but is a mitigation measure to decrease the frequency at which the error can occur.  
345 Additionally, the return to science mode sequence was updated on 27 May 2021 to further  
346 decrease the frequency of the error.

### 347 **3.4 Version 13: Ocean Weak Spots**

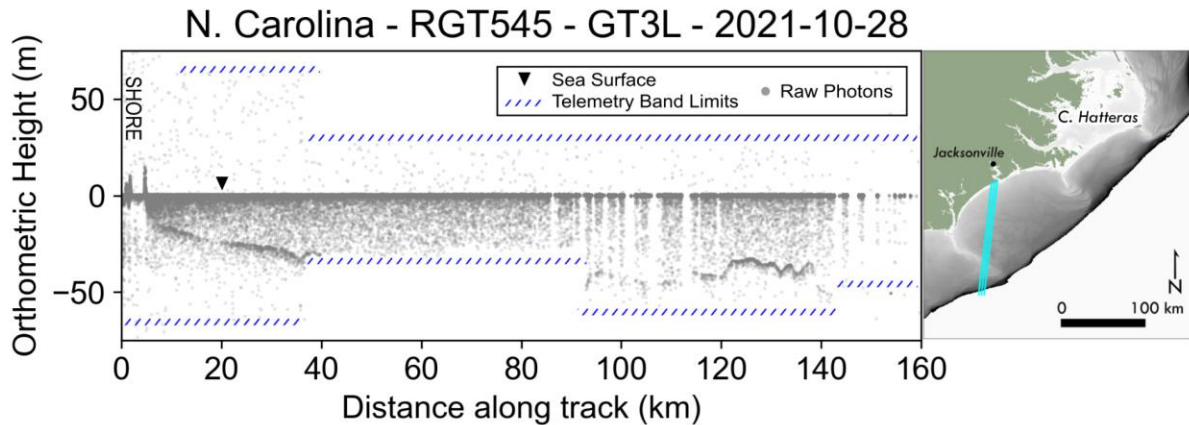
348 Prior to the Version 13 updates, weak spot ocean data was telemetered only when the  
349 Alternate Knobs were in use. Users of the Ocean Elevation Along-track Data Product (ATL12)  
350 found that weak spot returns have a sufficient signal-to-noise ratio to detect the ocean surface  
351 (Yu et al. 2021) and requested weak beam data to be consistently downlinked over the ocean.  
352 The utility of weak spot ocean data is further supported by the routine use in ICESat-2  
353 calibration scans which support spacecraft pointing and geolocation accuracy assessments  
354 (Luthcke et al. 2021). In the Knobs parameter files, the telemetry knobs for weak spot ocean

355 conditions were adjusted to downlink data when a Major Frame (nominally 200 pulses) or Super  
356 Frame (nominally 1000 pulses) signal is found. If no signal is found, then no data for weak spots  
357 is downlinked to minimize any increase in data volume. Note that the changes made in Version  
358 13 do not extend the telemetry bands for bathymetry that were introduced in Version 10 for the  
359 strong spots. Version 13 parameters became operational on 1 June 2021.

### 360 **3.5 Version 14: Coastline Bathymetry**

361 The increased ocean telemetry bands in Version 10 reduce bathymetry clipping in the  
362 open ocean, but that did not mitigate all of the instances of missing or clipped bathymetry data  
363 along coastlines. Figure 4 shows an example off the coast of North Carolina where the receiver  
364 algorithms set the telemetry band limits based on the land parameters, resulting in a loss of  
365 bathymetry. Because the on-board SRM can have multiple surface types in a single tile it  
366 prioritizes land over ocean when both are present in a SRM tile. As mentioned previously, the  
367 surface type dictates the level of vertical padding parameters for the telemetered data. Telemetry  
368 bands along coastlines therefore use the adjacent land parameters and, in some cases, lack the  
369 extended depth applied to the ocean telemetry bands because of the low relief values in the  
370 DRM.

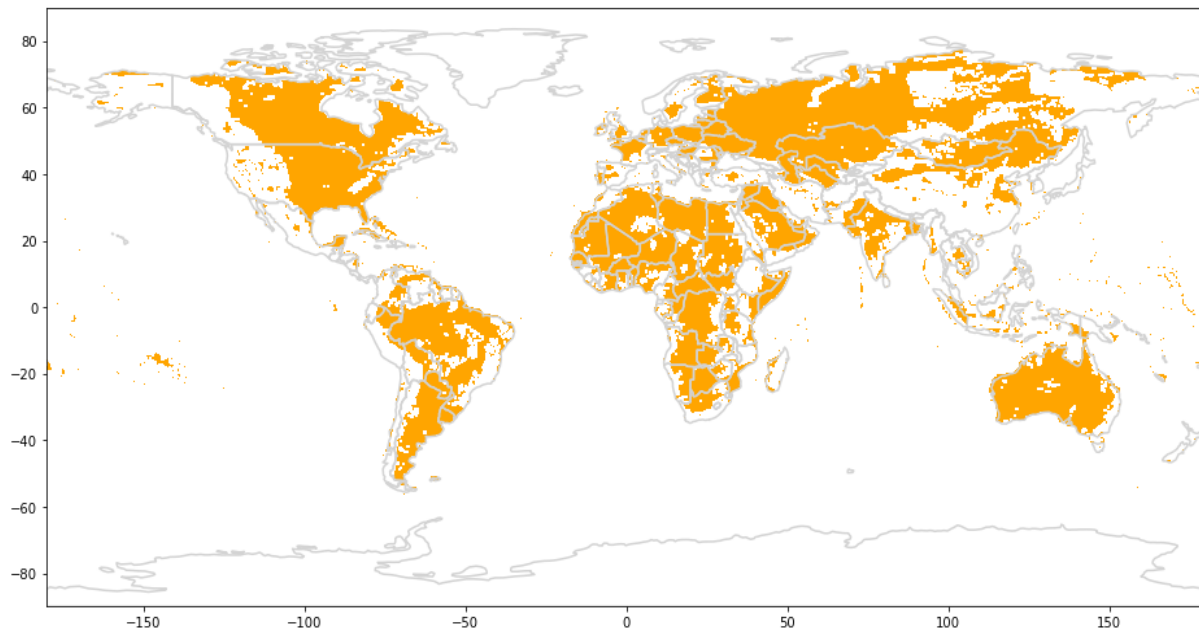
371



372  
 373 Figure 4. Bathymetric data loss after ocean telemetry band enhancements (v10) due to  
 374 prioritization of land in the on-board SRM, near the coast of North Carolina. Until 90 km along  
 375 track, the telemetry band parameters associated with land are in use when calculating the  
 376 telemetry band limits. (used with permission from Dietrich et al., 2023)  
 377

378 To correct the telemetry band settings in coastal areas two important considerations had  
 379 to be considered, the potential increases in data volume and reducing the likelihood of Did Not  
 380 Finish Major Frame (DNF MF) conditions (data transfer errors from the PCE cards). To create  
 381 the desired telemetry bands for coastal areas, the minimum padding over land for the strong spots  
 382 was increased by 30 m to approximately 54 m. This padding applies to all land areas with a  
 383 DRM relief value of 189 meters or less, highlighted in orange in Figure 5. The increase in the  
 384 minimum land padding reduces bathymetry clipping along coastlines where the SRM has not yet  
 385 switched from land to ocean. The changes are not applied to the weak spots, to remain consistent  
 386 with the previous ocean updates for capturing bathymetry (Version 10 and 13). These updates  
 387 became operational on-orbit on 1 December 2022. After this date, PCE1 and PCE3 each required  
 388 resetting. The resets result in gaps in Version 14 usage starting on 29 December 2022 for PCE1  
 389 and 2 February 2023 for PCE3. Version 14 became the permanent nominal parameters on all  
 390 PCEs on 6 February 2023.

391



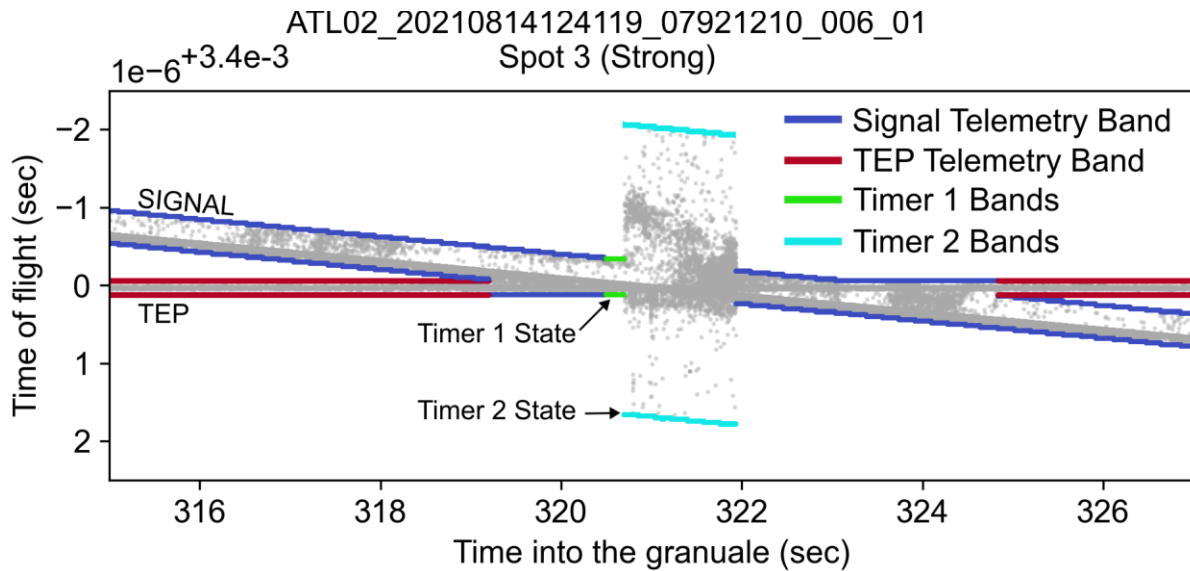
392  
393 Figure 5. Map of DRM tiles where the increased land padding is applicable. These tiles have a  
394 relief range of 0 to 189 meters.  
395

## 396 4. Results and Discussion

### 397 4.1 Version 08

398 Updates to the Knobs files in Version 08 mitigate the potential loss of data when the TEP  
399 crosses the ocean or sea ice surface due to the receiver algorithms' exclusion of the region about  
400 the TEP when searching for signal. When an ocean or sea ice surface enters the TEP region, the  
401 receiver algorithms enter the no-signal state and the updated Knobs are configured to continue  
402 telemetering the data using the no-signal state parameters. Figure 6 shows an example of the TEP  
403 crossing a sea ice surface. The Version 08 Knobs settings produce telemetry bands that  
404 successfully capture both the TEP and the surface as they intersect without any data clipping.  
405 When the surface enters the TEP region, the receiver algorithms first go into the no-signal timer1  
406 state and telemeter 10 Major Frames centered about the last known signal. After timer1  
407 concludes, the receiver algorithms switch to the no-signal timer2 state and telemeter bands that

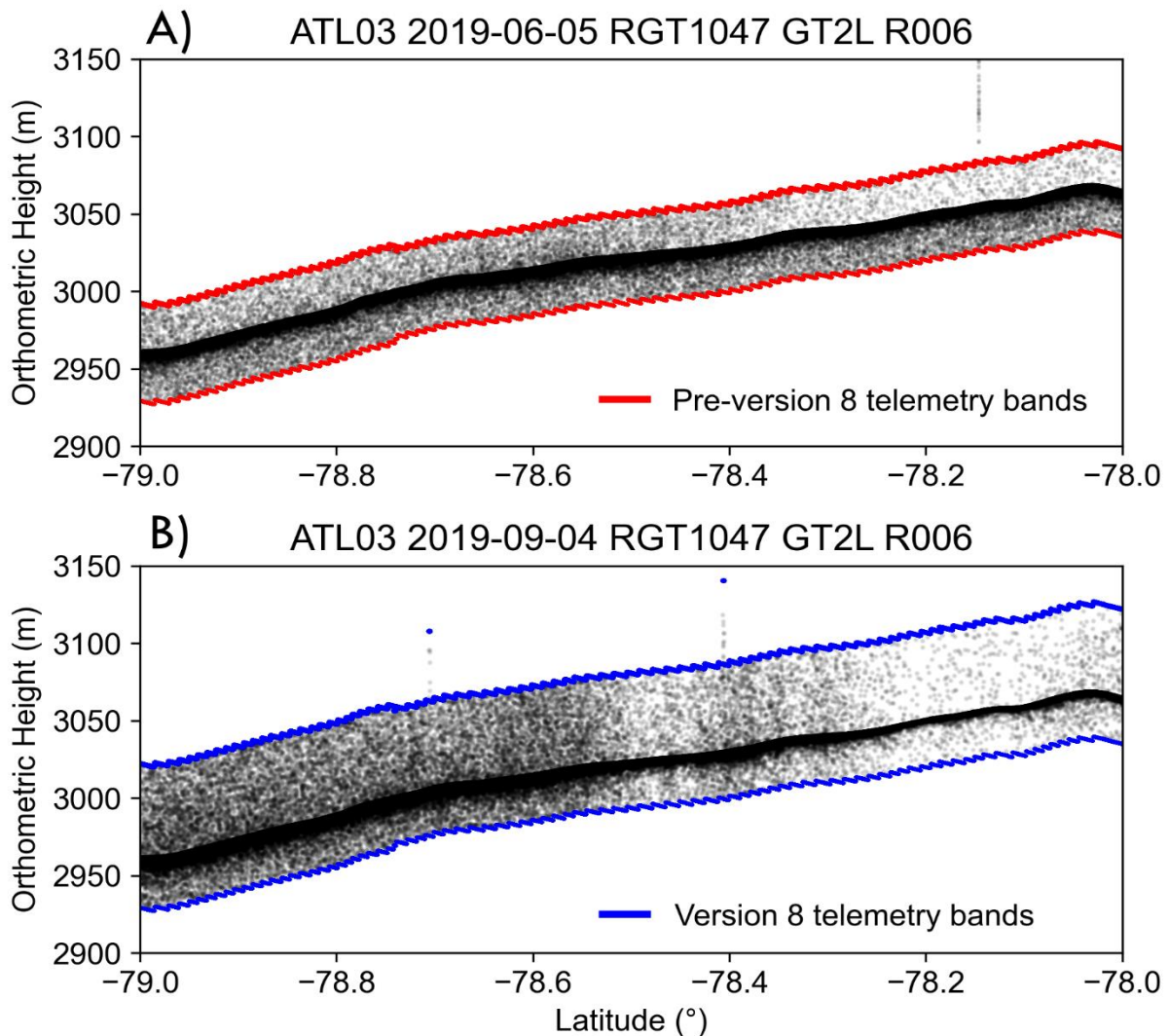
408 span the entire range window, ensuring surface is contained within the telemetry band. Timer2  
 409 concludes once a signal is found outside the TEP region. It is possible that both TEP and clouds,  
 410 or other noise features, are present in the range window. In such cases, noise features may be  
 411 selected as signal to be telemetered along with the TEP, and surface signals may be missed.  
 412



413  
 414 Figure 6. Example showing how the Version 8 changes for how the telemetry bands are  
 415 calculated for areas containing surface signal and TEP convergence.  
 416

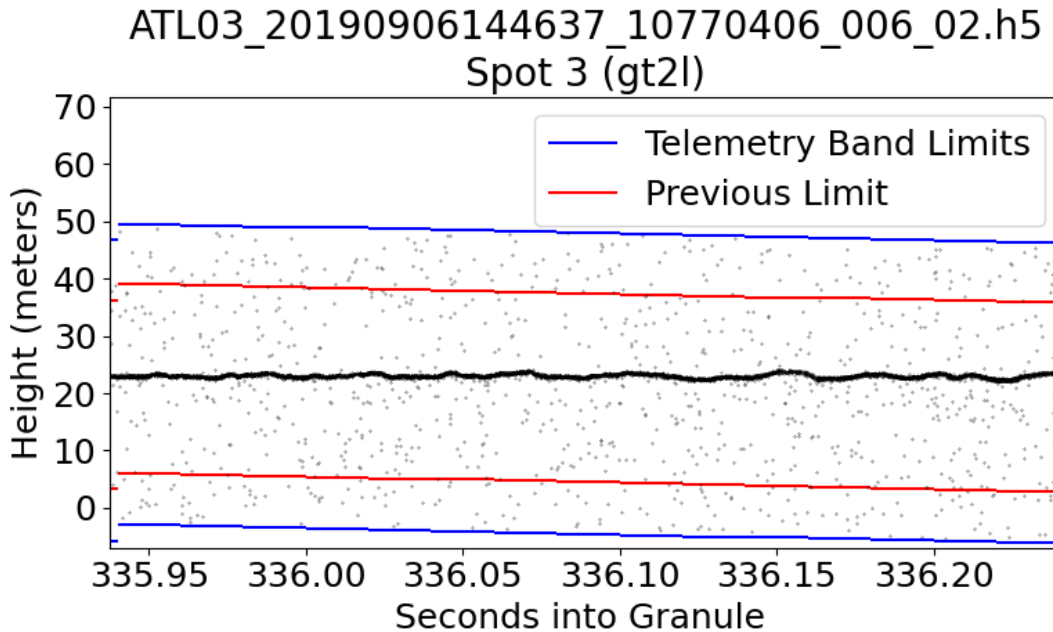
417 As the telemetry bands containing the surface signal (blue) and the telemetry bands containing  
 418 the TEP (red) converge, they first are combined into one telemetry band for each Major Frame  
 419 until the TEP is close enough to trigger the no-signal states, as shown in Figure 6. For ten Major  
 420 Frames the telemetry bands in the no-signal timer1 state (green) which are centered on the last  
 421 known signal location followed by over one second worth of the telemetry bands in the no-signal  
 422 timer2 state (cyan), which are centered within the range window. The telemetry bands go back to  
 423 a combined TEP and signal band once the signal is sufficiently out of the TEP region until they  
 424 are far enough apart to be telemetered separately.

425           The second update in Version 8 increased the telemetry band padding and offset  
426 parameter updates in the ST files for land ice and sea ice to increase the above surface portion of  
427 the telemetry band to better capture blowing snow. Blowing snow is an important component to  
428 understanding surface-atmosphere energy flux particularly in the polar regions (Herzfeld et al.  
429 2021) and this parameter change accommodates further investigations into these processes. All  
430 land ice and sea ice telemetry bands after the Version 08 update have an additional 30 meters in  
431 vertical width applied above the surface telemetry band limit, leaving the below surface limit  
432 unchanged, as described in Section 2. The total height above the surface in the telemetry band  
433 varies based on the relief value in the DRM. Figure 7 shows data from a portion of the same  
434 reference ground track in Antarctica (land ice) before and after Version 08 is made operational.  
435 The range in telemetry band widths increased by 30 meters, from 57 - 63 meters to 87 - 93  
436 meters. The surface is no longer centered in the telemetry band in Figure 7B since the additional  
437 30 meters of padding is expressed in the upper telemetry band limits.



438  
 439 Figure 7. Areas of blowing snow in Antarctica before (A) and after (B) the Version 08 updates  
 440 become operational. (A) On June 5, 2019, blowing snow is captured within the telemetry bands,  
 441 which have a vertical width ranging from approximately 57 to 63 meters. The surface signal is  
 442 centered within the telemetry bands, resulting in approximately 29.5 to 31.5 meters above the  
 443 surface available to capture blowing snow. (B) On September 4, 2019, additional blowing snow  
 444 is captured within the telemetry bands. The Version 08 updates produce telemetry bands with a  
 445 vertical width ranging from 87 to 93 meters with the additional 30 meters only applied to above  
 446 the surface. This results in approximately 59.5 to 61.5 meters of space above the surface to  
 447 capture blowing snow.  
 448

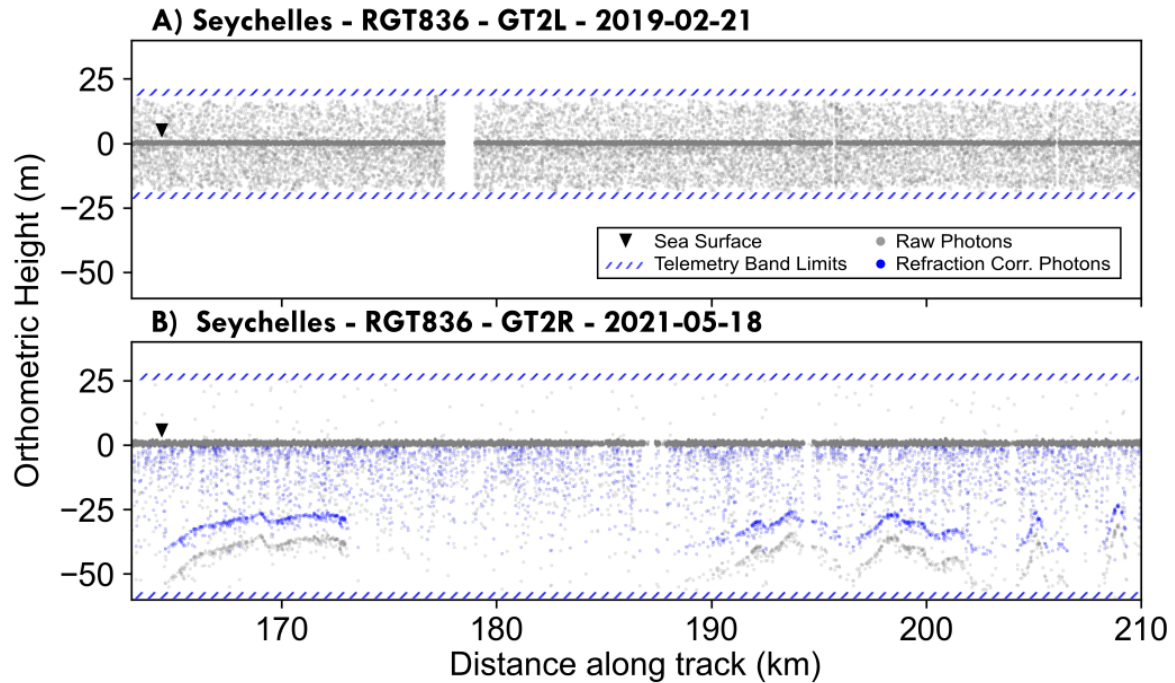
449 The third update implemented in Version 8 included small adjustments to telemetry  
 450 bands for the ocean surface type. The telemetry band padding parameter was increased to create  
 451 a total vertical band height of 48 m in vertical height ( $\pm 24$  m around the signal) (Figure 8).



452  
453 Figure 8. Telemetry over the ocean after the increase to the ocean telemetry band padding  
454 parameters. The Version 08 telemetry bands (blue) span a vertical width of ~51 meters, gaining  
455 ~10 meters both above and below the surface compared to the telemetry band limits prior to  
456 Version 08 (red).  
457

#### 458 **4.2 Version 10**

459 By extending the strong spot telemetry bands over ocean to 54 meters below the surface,  
460 bathymetry previously excluded in the data can now be captured. More specifically, potential  
461 bathymetry that falls below the previous telemetry band lower limit of 24 meters below the  
462 surface to the updated lower limit of 54 meters is now included in the downlinked data. Figure 9  
463 shows an example near the Seychelles where potential bathymetry is captured in the extended  
464 portion of the telemetry band. See Dietrich et al. (Dietrich et al. 2023) for additional details and  
465 examples.



466 Figure 9. Telemetry bands for reference ground track (RGT) 0836 in the Seychelles. a) illustrates  
 467 the telemetry bands before the Version 10 update showing no bathymetry. b) highlights the  
 468 expanded telemetry bands of Version 10 and the newly available reef bathymetry that was  
 469 previously not recorded (used with permission from Dietrich et al., 2023).  
 470  
 471

### 472 4.3 Version 11

473 The range window settings in Version 08 introduced, at times, large differences in the  
 474 range window starts of strong-weak pairs for PCEs 1 and 2. These differences are often on the  
 475 order of 2 kilometers or more. As described above, this condition increases the likelihood of  
 476 Tx/Rx slips. The range window adjustments in Version 11 reduce the differences in range  
 477 window starts to an average of a few meters or less, consistent with measurements for PCE 3.

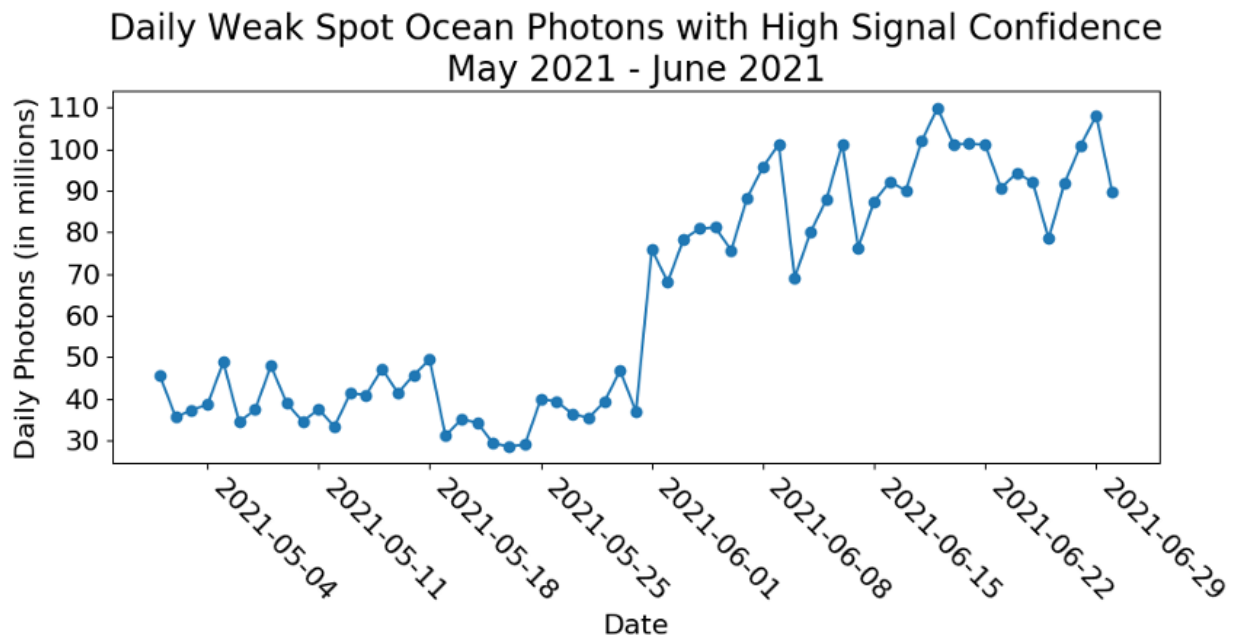
478 The Version 11 mitigation successfully reduced the conditions favorable for TxRx slips  
 479 introduced in Version 08. In Versions 08 through 10, TxRx slips occurred in 1,759 granules, or  
 480 1.54% of data over ~1.5 years. After the Version 11 update, TxRx slips occurred in just 314  
 481 granules, or 0.15% of data over more than 2.5 years as of this writing. Note that these figures  
 482 consider only the most common TxRx slip type, corrected in ATL02 (A. Martino, Field, and

483 Ramos-Izquierdo 2020).

#### 484 **4.4 Version 13**

485 Version 13 became operational on June 1, 2021, greatly increasing the amount of weak  
486 spot data available over the open oceans. Figure 10 shows the daily number of weak spot, ocean  
487 photons with high signal confidence in ATL03 (Neumann et al. 2019) for 1 May and 31 June  
488 2021, with a distinct jump on June 1, 2021 when Version 13 became operational. The ATL03  
489 weak spot, ocean data for May 2021 were data that were collected when the Alternate Knobs are  
490 in use (17 ocean scans, 8 round-the-world scans, and parts of the 42 ocean targets of opportunity  
491 (TOOs)) and times when the on-board SRM classification of ocean does not align with the  
492 ATL03 surface type classification. Because June 2021 has only one additional ocean scan and  
493 round-the-world scan, the increase in high signal confidence weak spot, ocean data can be  
494 attributed to the Version 13 parameter update. The addition of weak spot, ocean telemetry  
495 increases its fraction of the total data telemetered by approximately 1%. This small increase in  
496 percentage of data telemetered is expected due to the small size of the telemetry band (48 meters)  
497 and the reduced photon rate for weak-spots.

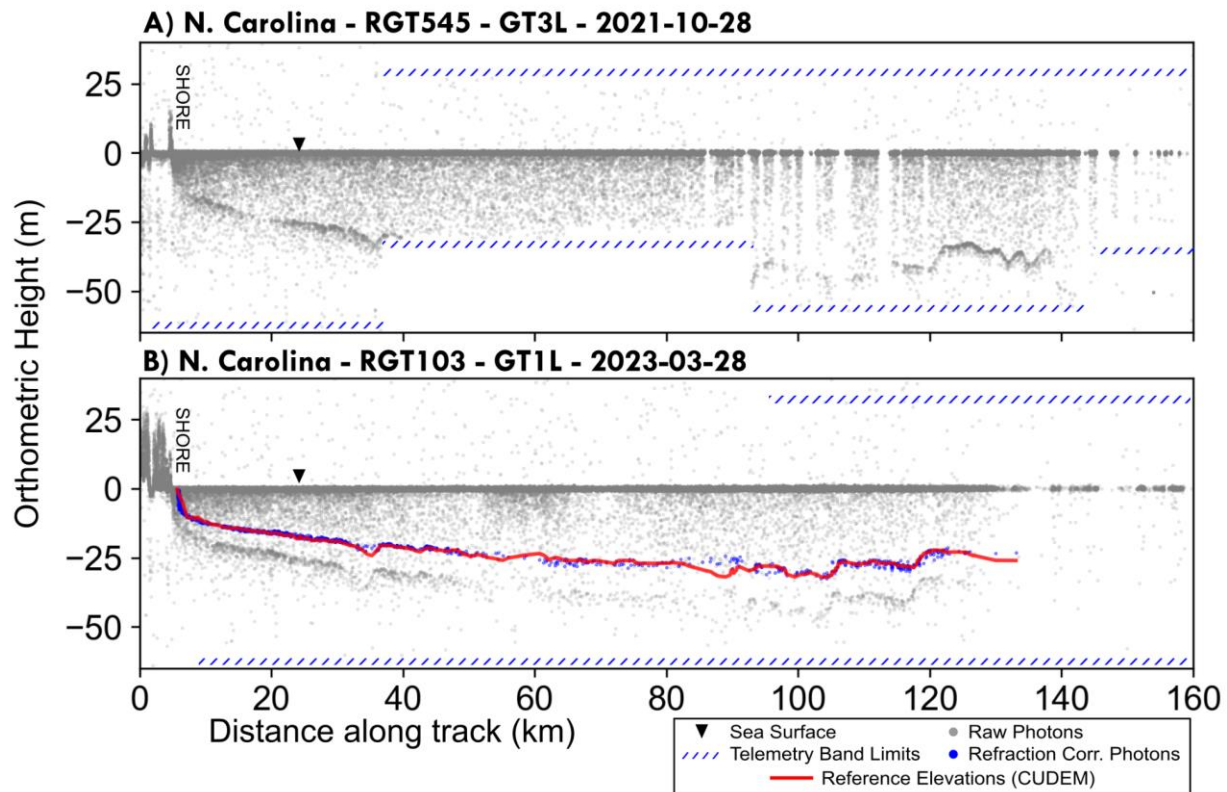
498 A recent example of the utility of using the weak beam data is the recovery of ocean  
499 wave characteristics, particularly nearshore where the dynamics are more complex.  
500 Understanding wave direction and the overall geometry of wave motion is only possible with the  
501 correlation of signal between two beams, in this case a pair (Dietrich, Magruder, and Holwill  
502 2023). It is anticipated that the inclusion of the weak spot will foster more science discovery  
503 moving forward as the mission accumulates data in relevant locations and extends coverage.



504  
 505 Figure 10. Daily sum of high signal weak spot, ocean photons in ATL03 from 05/01/2021 to  
 506 06/30/2021. The step increase in weak spot, ocean signal photons apparent on 06/01/2021 is due  
 507 to the Version 13 update becoming operational.  
 508

509 **4.5 Version 14**

510 The majority of the bathymetry potentially observable by ICESat-2 falls along coastlines  
 511 where the receiver algorithms set the telemetry band limits based on the parameters  
 512 corresponding to land surface type. The Version 10 updates include only parameters  
 513 corresponding to ocean surface type, so a large portion of potential bathymetry was not captured  
 514 by those updates. The Version 14 updates extend the land telemetry bands to at least as deep as  
 515 the ocean bands for areas that have a relief value less than or equal to 189 meters from the DRM.  
 516 Figure 11b shows the effect of the version 14 updates compared to the previous band limits  
 517 (Figure 11a and Figure 4). See Dietrich et al. (Dietrich et al. 2023) for a detailed study on how  
 518 much additional potential bathymetry the Version 14 and Version 10 updates provide.



519  
 520 Figure 11. Newly available bathymetry off the coast of North Carolina, USA after the Version 14  
 521 update. a) Previous telemetry band limits highlighting the clipped bathymetry caused by the  
 522 switching from land to ocean surface parameters and b) newly available continuous bathymetric  
 523 profile made possible by the consistent lower telemetry band limit of -54 meters below the  
 524 surface. Refraction corrected photon elevations are shown in blue with a comparison to NOAA  
 525 CUDEM elevations. (used with permission from Dietrich et al., 2023)  
 526

527 **6. Conclusions**

528 The ICESat-2/ATLAS receiver algorithms have had several updates since the launch of  
 529 the satellite in 2018. These modifications were motivated by a desire to optimize (further) the  
 530 science that the ICESat-2 measurements are able to facilitate and also to mitigate some  
 531 operational issues. This paper is a result of many scientists and engineers evaluating the icesat-2  
 532 data and highlights the exceptional response of the ICESat-2 project office to providing the  
 533 scientific community the quality of data that meets multi-disciplinary standards despite not being  
 534 part of the prime mission objectives. It is expected that these new adjustments and

535 accommodations will allow for enhanced research and discovery in many areas of Earth science.  
536 The software changes onboard were possible because of the careful planning and insight of the  
537 ATLAS engineers to enable adjustments to the quantity and quality of signals collected. ICESat-  
538 2 is an example of adaptability and resilience on-orbit to ensure that the mission is optimized for  
539 data collection that maximizes the scientific return.

#### 540 **Acknowledgments**

541 The authors wish to thank the ICESat-2 Project Science Office for the support as well as  
542 the NASA HQ support under grant #80NSSC23K0044. We also thank Alvaro Ivanoff for the  
543 data volume statistics around the Version 13 update and related figure.

#### 544 **Data Availability**

545 All data used in this publication is publicly available from the National Snow and Ice  
546 Data Center (<https://nsidc.org/>) from ATL02 and ATL03 ICESat-2 data products.

#### 547 **References**

- 548 Dietrich, James, Lori Magruder, and Matthew Holwill. 2023. "Monitoring Coastal Waves with  
549 ICESat-2." *Journal of Marine Science and Engineering* In pre-print. [https://doi.org/Doi:  
550 10.20944/preprints202310.1185.v1](https://doi.org/Doi:10.20944/preprints202310.1185.v1).
- 551 Dietrich, James, Ann R Rackley Reese, Aimée Gibbons, Lori A. Magruder, and Christopher  
552 Parrish. 2023. "Analysis of ICESat-2 Data Acquisition Algorithm Parameter  
553 Enhancements to Improve Worldwide Bathymetric Coverage." Preprint. Preprints.  
554 <https://doi.org/10.22541/essoar.169447414.45310708/v1>.
- 555 Herzfeld, Ute, Adam Hayes, Stephen Palm, David Hancock, Mark Vaughan, and Kristine  
556 Barbieri. 2021. "Detection and Height Measurement of Tenuous Clouds and Blowing  
557 Snow in ICESat-2 ATLAS Data." *Geophysical Research Letters* 48 (17).  
558 <https://doi.org/10.1029/2021GL093473>.
- 559 Jarvis, A., Hannes Reuter, Andy Nelson, and Edith Guevara. 2008. "Hole-Filled SRTM for the  
560 Globe Version 3, from the CGIAR-CSI SRTM 90m Database." *See Http://Srtm. Csi.  
561 Cgiar. Org*, January.
- 562 Leigh, Holly W., Lori A. Magruder, Claudia C. Carabajal, Jack L. Saba, and Jan F. McGarry.  
563 2015. "Development of Onboard Digital Elevation and Relief Databases for ICESat-2."  
564 *IEEE Transactions on Geoscience and Remote Sensing* 53 (4): 2011–20.  
565 <https://doi.org/10.1109/TGRS.2014.2352277>.
- 566 Luthcke, S. B., T. C. Thomas, T. A. Pennington, T. W. Rebold, J. B. Nicholas, D. D. Rowlands,  
567 A. S. Gardner, and S. Bae. 2021. "ICESat-2 Pointing Calibration and Geolocation

- 568 Performance.” *Earth and Space Science* 8 (3). <https://doi.org/10.1029/2020EA001494>.
- 569 Magruder, Lori, Kelly Brunt, Thomas Neumann, Bradley Klotz, and Michael Alonzo. 2021.
- 570 “Passive Ground-Based Optical Techniques for Monitoring the On-Orbit ICESat-2
- 571 Altimeter Geolocation and Footprint Diameter.” *Earth and Space Science* 8 (10).
- 572 <https://doi.org/10.1029/2020EA001414>.
- 573 Magruder, Lori, Thomas Neumann, and Nathan Kurtz. 2021. “ICESat-2 Early Mission Synopsis
- 574 and Observatory Performance.” *Earth and Space Science* 8 (5).
- 575 <https://doi.org/10.1029/2020EA001555>.
- 576 Magruder, Lori, Tom Neumann, Nathan Kurtz, and Tyler Sutterley. 2024. “The Ice, Cloud and
- 577 Land Elevation Satellite-2: Meeting the Prime Mission Science Requirements.” *Remote*
- 578 *Sensing of Environment*, no. In review.
- 579 Markus, Thorsten, Tom Neumann, Anthony Martino, Waleed Abdalati, Kelly Brunt, Beata
- 580 Csatho, Sinead Farrell, et al. 2017. “The Ice, Cloud, and Land Elevation Satellite-2
- 581 (ICESat-2): Science Requirements, Concept, and Implementation.” *Remote Sensing of*
- 582 *Environment* 190 (March): 260–73. <https://doi.org/10.1016/j.rse.2016.12.029>.
- 583 Martino, A. J., M. R. Bock, R. L. Jones III, T. A. Neumann, D. Hancock, P. W. Dabney, and C.
- 584 E. Webb. 2019. “ATLAS/ICESat-2 L1B Converted Telemetry Data, Version 1.” NASA
- 585 National Snow and Ice Data Center Distributed Active Archive Center.
- 586 <https://doi.org/10.5067/ATLAS/ATL02.001>.
- 587 Martino, Anthony, Christopher T Field, and Luis Ramos-Izquierdo. 2020. “ICESat-2/ATLAS
- 588 Instrument Linear System Impulse Response.” Preprint. Geophysics.
- 589 <https://doi.org/10.1002/essoar.10504651.1>.
- 590 Martino, Anthony J., Thomas A. Neumann, Nathan T. Kurtz, and Douglas McLennan. 2019.
- 591 “ICESat-2 Mission Overview and Early Performance.” In *Sensors, Systems, and Next-*
- 592 *Generation Satellites XXIII*, 11151:68–77. SPIE. <https://doi.org/10.1117/12.2534938>.
- 593 McGarry, J. F., C. C. Carabajal, J. L. Saba, A. R. Reese, S. T. Holland, S. P. Palm, J.-P. A.
- 594 Swinski, J. E. Golder, and P. M. Liiva. 2021. “ICESat-2/ATLAS Onboard Flight Science
- 595 Receiver Algorithms: Purpose, Process, and Performance.” *Earth and Space Science* 8
- 596 (4). <https://doi.org/10.1029/2020EA001235>.
- 597 Neumann, Thomas A., Anthony J. Martino, Thorsten Markus, Sungkoo Bae, Megan R. Bock,
- 598 Anita C. Brenner, Kelly M. Brunt, et al. 2019. “The Ice, Cloud, and Land Elevation
- 599 Satellite – 2 Mission: A Global Geolocated Photon Product Derived from the Advanced
- 600 Topographic Laser Altimeter System.” *Remote Sensing of Environment* 233 (November):
- 601 111325. <https://doi.org/10.1016/j.rse.2019.111325>.
- 602 Parrish, Christopher E., Lori A. Magruder, Amy L. Neuenschwander, Nicholas Forfinski-
- 603 Sarkozi, Michael Alonzo, and Michael Jasinski. 2019. “Validation of ICESat-2 ATLAS
- 604 Bathymetry and Analysis of ATLAS’s Bathymetric Mapping Performance.” *Remote*
- 605 *Sensing* 11 (14): 1634. <https://doi.org/10.3390/rs11141634>.
- 606 Schutz, B. E., H. J. Zwally, C. A. Shuman, D. Hancock, and J. P. DiMarzio. 2005. “Overview of
- 607 the ICESat Mission.” *Geophysical Research Letters* 32 (21): L21S01.
- 608 <https://doi.org/10.1029/2005GL024009>.
- 609 Simard, Marc, Naiara Pinto, Joshua B. Fisher, and Alessandro Baccini. 2011. “Mapping Forest
- 610 Canopy Height Globally with Spaceborne Lidar.” *Journal of Geophysical Research* 116
- 611 (G4): G04021. <https://doi.org/10.1029/2011JG001708>.
- 612 Smith, Ben, Helen A. Fricker, Alex S. Gardner, Brooke Medley, Johan Nilsson, Fernando S.
- 613 Paolo, Nicholas Holschuh, et al. 2020. “Pervasive Ice Sheet Mass Loss Reflects

614           Competing Ocean and Atmosphere Processes.” *Science* 368 (6496): 1239–42.  
615           <https://doi.org/10.1126/science.aaz5845>.  
616 Yu, Yao, David T Sandwell, Sarah T Gille, and Ana Beatriz Villas Bôas. 2021. “Assessment of  
617 ICESat-2 for the Recovery of Ocean Topography.” *Geophysical Journal International*  
618 226 (1): 456–67. <https://doi.org/10.1093/gji/ggab084>.  
619

1 **ICESat-2 Onboard Flight Receiver Algorithms: On-orbit Parameter Updates**  
2 **the Impact on Science Driven Observations**

3  
4 Lori Magruder<sup>1</sup>, Ann Rackley Reese<sup>2,3</sup>, Aimée Gibbons<sup>2,3</sup> James Dietrich<sup>1</sup> and Tom Neumann<sup>3</sup>

5 <sup>1</sup>Center for Space Research, University of Texas at Austin, Austin, TX.

6 <sup>2</sup>KBR, Greenbelt, MD

7 <sup>3</sup>NASA Goddard Space Flight Center, Greenbelt, MD

8  
9 Corresponding author: Lori Magruder<sup>†</sup> ([lori.magruder@austin.utexas.edu](mailto:lori.magruder@austin.utexas.edu))

10  
11 Key Points:

- 12 ● Since the 2018 ICESat-2 launch multiple updates have been made to the satellite's  
13 onboard flight receiver algorithm parameters to improve access and utility of the data for  
14 a multi-disciplinary science community
- 15 ● The adjustments have been primarily in the in the vertical telemetry window settings and  
16 have facilitated enhanced observations of blowing snow and increased detection  
17 opportunities of bathymetry in nearshore environments
- 18 ● The parameter changes have been made to mitigate data losses in certain situations and  
19 to advance science applications outside of the primary science objectives of the ICESat-2  
20 mission.

21

22 **Abstract**

23 The ICESat-2 (Ice, Cloud and Land Elevation Satellite-2) photon-counting laser altimeter  
24 technology required the design and development of very sophisticated onboard algorithms to  
25 collect, store and downlink the observations. These algorithms utilize both software and  
26 hardware solutions for meeting data volume requirements and optimizing the science achievable  
27 via ICESat-2 measurements. Careful planning and dedicated development were accomplished  
28 during the pre-launch phase of the mission in preparation for the 2018 launch. Once on-orbit all  
29 of the systems and subsystems were evaluated for performance, including the receiver  
30 algorithms, to ensure compliance with mission standards and satisfy the mission science  
31 objectives. As the mission has progressed and the instrument performance and data volumes  
32 were better understood, there have been several opportunities to enhance ICESat-2's  
33 contributions to earth observation science initiated by NASA and the ICESat-2 science  
34 community. We highlight multiple updates to the flight receiver algorithms, the onboard  
35 software for signal processing, that have extended ICESat-2's data capabilities and allowed for  
36 advanced science applications beyond the original mission objectives.

37 **Plain Language Summary**

38 NASA launched its second Earth observing laser altimeter in 2018 with mission objectives of  
39 collecting observations in support of Earth science as a window into climate change impacts on  
40 our planet. Pre-launch studies focused on specific instrument settings and on-board data  
41 processing to support the mission objectives without violating data volume constraints. Once the  
42 instrument was on-orbit and operational, evaluation of the algorithms for success in signal  
43 detection, signal finding, and signal telemetry was undertaken. In response to the evaluation,  
44 updates have been made to optimize the data provided by the mission.

45 **1. Introduction**

46 The Ice, Cloud and land Elevation Satellite-2 (ICESat-2) has been providing global height  
47 measurements to the scientific community since 2018. ICESat-2 has similar scientific objectives  
48 as its predecessor mission, ICESat (Schutz et al. 2005), with a focus on using satellite laser  
49 altimetry to support climate variable monitoring as a window to understanding Earth's response  
50 to a changing climate. The primary instrument onboard ICESat-2 is the Advanced Topographic  
51 Laser Altimetry System (ATLAS) and is one of the most technically advanced space-borne lidar  
52 for Earth Science to date (Martino et al. 2019). ATLAS is a photon-counting lidar, sensitive to  
53 single photon reflections from the surface of the Earth. The photon-counting technology  
54 facilitates the use of lower laser energy, creating a scenario where multiple beams and higher  
55 laser repetition rates allow for greater spatial coverage and higher spatial resolution, both of  
56 which were implemented improvements based on operational realizations identified by the  
57 predecessor mission (ICESat) (Markus et al. 2017; Magruder et al. 2021). The high repetition rate  
58 (10kHz) provides higher along-track spatial resolution and the capability to capture fine scale  
59 features on the surface in time and space to meet requirements associated with dynamic  
60 processes in our Polar Regions. The multiple beam configuration allows for the discrimination  
61 between surface slope and true elevation change in the case of repeat measurements (Smith et al.  
62 2020). ICESat-2 mission requirements are described by Markus et al. (2017) and successful  
63 completion of the requirements is summarized in Magruder et al., 2024 (Magruder et al. 2024).  
64 The large data volume associated with a photon counting lidar was anticipated and the approach  
65 to onboard data management and signal processing techniques had to be altered from previous  
66 missions. It was understood and expected that ATLAS would exceed the normal X-band radio  
67 downlink capabilities and could require additional downlink station contacts (McGarry et al.

68 2021). The ICESat-2 Project Science Office (PSO) made the decision early in the pre-launch  
69 mission phase to focus on reducing the data volume onboard via processing algorithms and then  
70 determine if there was a need for more ground station access. The onboard algorithms that  
71 comprise the flight software (FSW) were designed to provide a sophisticated means for signal  
72 finding and data reduction. These functions are performed through inventive use of onboard  
73 signal processing, databases, and telemetry window selection across the diversity of global  
74 environments and surface types (Leigh et al. 2015; McGarry et al. 2021). Each component of the  
75 comprehensive FSW was created around the idea of having flexible parameterization to  
76 accommodate on-orbit adjustments, changes, and updates as the mission matured and discoveries  
77 of future, unanticipated needs are identified through the prime mission lifetime and into the  
78 extended mission timeline.

79 The majority of the data volume acquired by ATLAS during each orbit and between downlink  
80 opportunities occurs during daylight hours. This accumulation is due to the nature of photon-  
81 counting systems, as ATLAS is susceptible to solar background noise entering the system at the  
82 same wavelength to the ATLAS laser (532 nm). During the day the ambient background noise  
83 can exceed 10 MHz, which creates the need for noise mitigation processing in order to not  
84 violate the telemetry constraints associated with downlink bandwidth limitations. Whether noise  
85 or signal, ATLAS detects and records the time of arrival for every received photon creating a  
86 disparity among detection types based on an extremely low signal to noise ratio (Anthony J.  
87 Martino et al. 2019). These challenges created a need for optimizing onboard techniques for  
88 ensuring capture of the surface signal without possible data losses associated with overloading  
89 downlink opportunities.

90 The overarching requirements for the onboard receiver algorithm FSW are: 1) Keep the average

91 daily science telemetry data volume below 577.4 Gb/day, 2) Use the real time position and  
92 attitude solutions to guide the surface signal finding within 2 km horizontally and 250 m  
93 vertically for off-nadir angles between  $0^\circ$  and  $\pm 5^\circ$  (with capabilities up to  $\pm 10^\circ$  off-nadir pointing  
94 after July 20, 2023), and 3) Select/find surface signal at least 90% of the time in regions of  
95 optically thin cloud cover, but not constrained by surface reflectivity, topography or solar  
96 elevation angle.

97 The utility of the receiver algorithms is to meet the volume constraints while capturing a  
98 complete and accurate altimetry signal of surface elevations. This is accomplished through  
99 several complementary functions that involve signal processing and functions that use a set of  
100 onboard databases of Earth elevations and topographic relief to inform where to look for true  
101 surface signal. Once the approximate surface is determined, the algorithm can align an  
102 appropriate telemetry window to ensure appropriate signal retention and successful data  
103 downlink. Comprehensive descriptions of the onboard receiver algorithm operations and  
104 capabilities are well described in the previous publications (Leigh et al. 2015; McGarry et al.  
105 2021) but will be mentioned in the subsequent sections for completion.

106 This article provides an overview of changes that have been made to the ICESat-2 FSW and  
107 receiver algorithms since launch. The FSW updates have been made to enhance ICESat-2's  
108 usefulness across a wide range of earth observation topics, including measurements of blowing  
109 snow and coastal bathymetry. We provide an overview of FSW and then discuss each update and  
110 the impact on ICESat-2 data products and the applications to earth observation science.

## 111 **1.1 Signal processing**

112 The Photon Counting Electronics (PCE) cards operate on each pair of strong and weak  
113 beams. The PCEs record the transmit and receive times of photons for each ATLAS pulse. Using

114 the transmit and receive times the time of flight (TOF) can be calculated and used to generate  
115 coarse range values that are then used to produce histograms of photon arrival times. The  
116 histograms are aggregates of 200 consecutive laser shots, corresponding to an along-track  
117 distance of 140 m (or 0.02 s) (McGarry et al. 2021). The flight software uses the histograms to  
118 perform initial signal and background rate estimates to inform data downlink criteria.

119 For two of the three strong beams a portion of the laser energy is redirected back to the  
120 receiver channel instead of being transmitted to the surface. This laser pickoff, called the TEP  
121 (Transmitted Echo Path), is fixed relative to the time of laser fire from which it was generated,  
122 with the primary pulse peak time-of-flight around 18-19 ns. The TEP is only recorded when it  
123 falls within the range window (RW) for a given laser fire but allows the instrument to record the  
124 shape of the outgoing laser pulse, providing a means to monitor the health and data quality of  
125 ATLAS. It also facilitates the identification of deteriorated conditions, such as transmit/receive  
126 pulse slips and fine count swaps. The most recent TEP photons meeting certain quality criteria  
127 are carried onto the ATL03 data product as ancillary information (Neumann et al. 2019).

## 128 **1.2 Databases and Telemetry window selection**

129 The next signal finding step is performed on the detected photons that exist within the  
130 determined range window through a combination of software and hardware approaches. The  
131 primary function of this step is to determine the appropriately sized vertical telemetry band that  
132 will encompass the surface photon reflections and limit excess data volume caused by noise  
133 photons and be telemetered down to ground stations for further processing. The telemetry band is  
134 defined as the vertical extent for which detected photons (signal and noise) are downlinked. The  
135 RW is ultimately determined by an onboard digital elevation model (DEM) that contains the  
136 minimum and maximum elevations globally. These elevation grids are indexed by latitude and

137 longitude and meet the requirement of 150 m ( $3\sigma$ ) accuracy (McGarry et al. 2021). The RW is  
138 constrained to a vertical maximum of 6 km that includes a  $\pm 250$  m height margin. To meet this  
139 requirement the onboard DEM is actually comprised of a tertiary grid system of varying  
140 resolutions ( $1^\circ \times 1^\circ$ ,  $0.25^\circ \times 0.25^\circ$ ,  $0.05^\circ \times 0.05^\circ$ ) to maintain that the relief (vertical distance  
141 between maximum and minimum elevation at a given geographical location) does not exceed  
142 5500 m. The baseline for where the expected surface elevation can be found within the vertical  
143 window is derived from the void-filled SRTM (Shuttle Radar Topography Mission) product  
144 released by the CGIAR-CSI (Consortium for Spatial Information; SRTM-CGIAR (Jarvis et al.  
145 2008)) for the mid-latitudes and other available DEMs outside of the SRTM latitudinal reach  
146 (e.g. Greenland Ice Mapping Project (GIMP), Bedmap2, Global Multi-resolution Terrain  
147 elevation Data (GMTED), and the Canadian Digital elevation Database (CDED)). The  
148 EGM2008 geoid is used to estimate the ocean surface elevations (Leigh et al. 2015).

149         The global relief database is the second type of database onboard ICESat-2. This DRM  
150 (digital relief model) establishes the elevation range surrounding the identified ground signal that  
151 is incorporated into the telemetry band calculation, along with padding and offset parameters.  
152 The DRM is assembled at a resolution of  $0.25^\circ \times 0.25^\circ$ , and contains the maximum relief values  
153 across two length scales (140 m and 700 m) (Leigh et al. 2015). The DRM relief values overlay  
154 the signal bin representing the perceived or apparent ground, helping ascertain the number of  
155 adjacent bins to incorporate into the downlink telemetry, aside from the signal bin itself. Failing  
156 to include the DRM relief values could result in the omission of ground and canopy signals in  
157 rugged and/or vegetated regions from the downlinked data. The DEM and DRM databases were  
158 enhanced by incorporating global vegetation heights obtained from Simard et al. (2011) (Simard  
159 et al. 2011).

160 The third type of database onboard ICESat-2 is the Surface Reference Mask (SRM) and, like the  
161 DRM, is at a resolution of  $0.25^\circ \times 0.25^\circ$ . The SRM classifies the surface type, as a means to  
162 define values of vertical (elevation) padding required for the telemetry window. This is used to  
163 accommodate (and mitigate) the uncertainties in the relief estimates and geolocation knowledge.  
164 The SRM also indicates if there is vegetation, and if there is coastline for each tile. The four  
165 possible surface types are land ice, sea ice, land, and ocean with precedence given in that order  
166 for mask cells that cover multiple surface types (McGarry et al. 2021).

## 167 **2. Materials and Methods**

168 As part of the ATLAS FSW, the receiver algorithms use several adjustable parameter  
169 files that allow modifications to the signal processing elements of the software to be updated  
170 without having to modify or update the underlying code of the FSW and receiver algorithms.  
171 Many of the parameters are determined as a function of either surface type, spot type (i.e. beam  
172 energy), or day or night conditions allowing for fine-tuned and discipline specific adjustments.  
173 The values are specified in a set of three parameter files. Each of the three onboard PCE  
174 detectors have an independent set of files, however all three PCE parameter files are  
175 synchronized to the same update version. The receiver algorithm parameter file types and their  
176 parameters that are frequently updated are described in the following sections.

### 177 **2.1 “Knobs” files (nominal and alternate parameters)**

178 The Knobs files contain parameters that allow control over the data volume by selecting  
179 content in the telemetry downlink and the conditions associated with when to telemeter data.  
180 Each PCE has a nominal Knobs file and an Alternate Knobs file. The nominal Knobs files are  
181 optimized for the main science objectives and keeping the data volume within the daily limit.  
182 The Alternate Knobs are used for those situations where the satellite is performing maneuvers

183 associated with ocean scans, round-the-world scans (Luthcke et al. 2021), and targets of  
184 opportunity (Magruder et al. 2021). The Alternate Knobs files create a configuration that  
185 continuously telemeters data regardless of surface type, time of day, or signal type. Only one  
186 Knobs file type is in use at a time for each PCE.

187         The telemetry “Knobs” parameters control what data to telemeter, or the content of the  
188 downlink. There are knobs for the numerous possible signal conditions, categorized by surface  
189 type, day or night acquisition, and spot strength (strong or weak). The No-signal Timer  
190 parameters count the number of consecutive Major Frames (nominally 200 laser pulses) to  
191 telemeter when no signal is identified by the receiver algorithms. There are two timer states,  
192 timer1 and timer2. The receiver algorithms enter the timer1 state when no signal is found for a  
193 major frame and the knobs are configured to still telemeter data. Timer1 currently varies from 10  
194 to 50 major frames, depending on the surface type. Timer2 begins when timer1 has expired and  
195 currently varies from 100 major frames to no expiration, depending on the surface type. The  
196 timer2 state generally consists of vertically larger telemetry bands. If timer2 expires then no data  
197 is selected to telemeter until signal is found again.

## 198         **2.2 PPR (Position, Pointing, and Range parameters)**

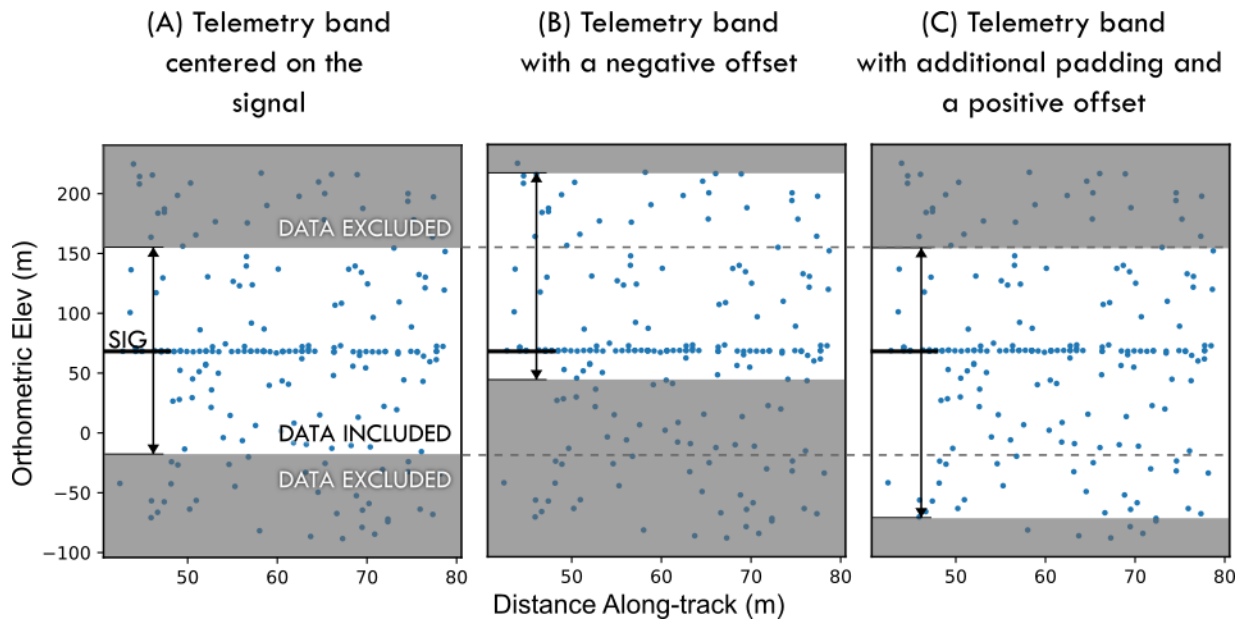
199         The PPR files contain parameters associated with calculating each spot location on Earth  
200 and setting the Range Window (search area to look for signal). The Range Window Minimum  
201 Width parameters define the minimum allowed vertical width of the range window. It can be set  
202 separately for each surface type, day or night, and strong or weak spot.

## 203         **2.3 ST (Signal and Telemetry parameters)**

204         The ST files contain parameters used in signal processing and calculating the vertical  
205 width of the telemetry bands. The telemetry band padding parameters define the amount of

206 margin to add in the calculation of the telemetry band width. The padding value is doubled and  
207 added to the scaled relief to account for uncertainties in the relief value. The relief comes from  
208 the onboard DRM and the scale factor is a parameter in the ST file. The padding parameters are a  
209 function of surface type, spot type and relief value. There are four ranges of relief (R) values ( $R$   
210  $\leq 189$  m,  $189$  m  $< R \leq 567$  m,  $567$  m  $< R \leq 1323$  m,  $1323$  m  $< R$ ) which specify the interval of  
211 padding to use. Generally, the padding values increase with each interval, except for ocean  
212 surface types.

213         The telemetry band offset and padding parameters define the position and shape of the  
214 telemetry band in vertical space (Figure 1). Offsets can be applied to shift the telemetry band up  
215 or down, a positive offset shifts the telemetry band down in vertical space and a negative offset  
216 shifts the telemetry band up in vertical space. An offset of 0 centers the telemetry band around  
217 the signal location. Padding is applied based on the onboard DRM values and increases the  
218 overall height of the telemetry band (symmetrically around the signal position). Offset and  
219 padding can be applied independently or in concert with each other to achieve the necessary  
220 telemetry band.



221  
 222 Figure 1. Diagram illustrating the different adjustments that are available when defining the  
 223 telemetry window. 200-photon returns are illustrated in each plot and data that would be  
 224 excluded (not downlinked) are shown in the gray boxes. (a) shows a normally centered telemetry  
 225 window around a signal (ground surface) at ~60 m elevation, (b) the window with the same  
 226 height as (a) with a negative offset applied to capture more data above the signal surface, and (c)  
 227 increased padding applied and a positive offset to increase the amount of data below the signal  
 228 surface while maintaining the height of the window limit above the signal.  
 229

### 230 3. Summary of on-orbit changes

231 Parameter file Versions 01 through 05 cover the work done in pre-launch simulated testing,  
 232 Integration and Testing (I&T), and observatory testing. ICESat-2 launched on 15 September  
 233 2018 operating on Version 06 parameter files (McGarry et al., 2020). Since launch, there have  
 234 been five version updates to the operational parameter files. As of this writing, ICESat-2 is  
 235 operating on Version 14. There are several file versions tested on-orbit or only in simulated  
 236 testing that were never made operational (07, 09 and 12). Table 1 has a summary of the testing  
 237 and operational timelines for each operational version since launch.

238  
 239

240

241 Table 1. Parameter file version test dates, test durations and operational start dates. Versions 07  
 242 and 09 were tested on-orbit, but never made operational. Version 12 was not tested on-orbit and is  
 243 therefore excluded from the table. \*Due to resetting of PCE1 and PCE3, there are gaps in usage of  
 244 v14: 29 Dec 22 - 6 Feb 23 for PCE1 and 2 Feb 23 - 6 Feb 23 for PCE3.

Version	Test Start Date	Test Duration (approx.)	Date Operational	Description
06	--	--	15 Sept 2018	Launch version
07	4 Apr 2019	4 hours	--	Data enhancements (TEP crossing signal) Corrected range window settings
08	9 May 2019	5 hours	3 Sept 2019	Data enhancements (TEP crossing signal, ocean, blowing snow) Corrected range window settings
09	25 Oct 2019	2 days	--	Data enhancements (lake bathymetry)
10	17 Nov 2020	2 weeks	27 Jan 2021	Data enhancements (ocean bathymetry)
11	16 Feb 2021	3.5 hours	12 Mar 2021	Error mitigation related to range windows
13	18 May 2021	5 hours	1 June 2021	Data enhancements (weak spot ocean)
14	1 Nov 2022	30 days	1 Dec 2022 *	Data enhancements (coastline bathymetry)

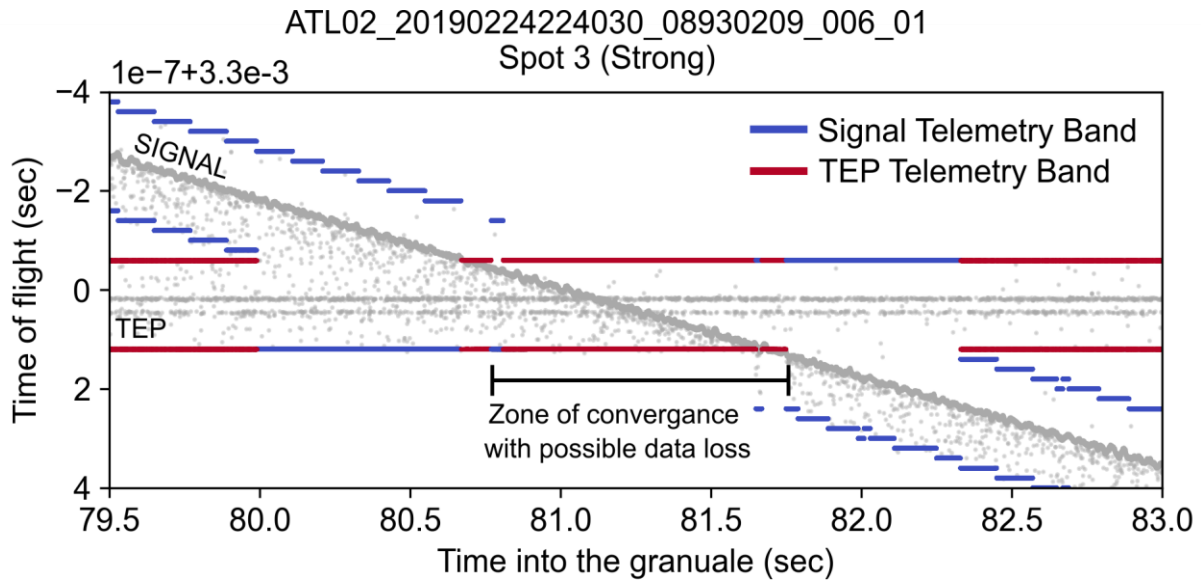
245

### 246 **3.1 Version 08: TEP Signal Crossing, Ocean and Blowing Snow Band Widths**

247 The first operational version revision of the parameter files is Version 08 was tested on  
 248 orbit in May 2019 and made operational on 3 September 2019. This version includes changes to  
 249 the Knobs, PPR, and ST files. Version 08 updates incorporated three major changes: 1)  
 250 mitigating the loss of data when the Transmitter Echo Path (TEP) is close to surface, which  
 251 reduced the range window widths for non-TEP photons to the nominal value 2) increasing  
 252 telemetry band widths to capture blowing snow and 3) increased telemetry band widths more  
 253 area around the open ocean surfaces.

254 The first Knobs file update mitigates data losses when the TEP is close to an ocean or sea  
 255 ice surface, shown in Figure 2 for the ocean. The nominal parameter settings tell the receiver

256 algorithms to ignore the area around the TEP (~27 meter vertical window) when searching for  
257 surface signal to avoid selecting the TEP as signal. This logic combined with the TEP  
258 approaching a flat surface can result in multiple Major Frames of missed surface data. In order to  
259 preserve signal data when the TEP intersects with the surface return, the Knobs parameters for  
260 the strong spots over ocean are turned on when no signal is found via the standard  
261 histogramming approach. The no-signal timer1 for both ocean and sea ice was reduced from 25  
262 Major Frames to 10 Major Frames and the no-signal timer2 is set to continuously telemeter data.  
263 By switching to the no-signal timer2 state sooner, the telemetry bands are set to the width of the  
264 range window ensuring both the TEP and surface are captured until there is sufficient distance  
265 between the TEP and surface, on the order of approximately 20 m for ocean and sea ice. This  
266 approximation allows for the established histogram bin size of ~12 m for ocean or sea ice surface  
267 signal and ~27 m for the TEP. Assuming the surface signal is in the middle of the bin (6 m on  
268 each side) and the TEP is in the middle of the bin (14 m on each side) the result is the 20 m  
269 estimate but in general the range is ~14 m to ~24 m.  
270



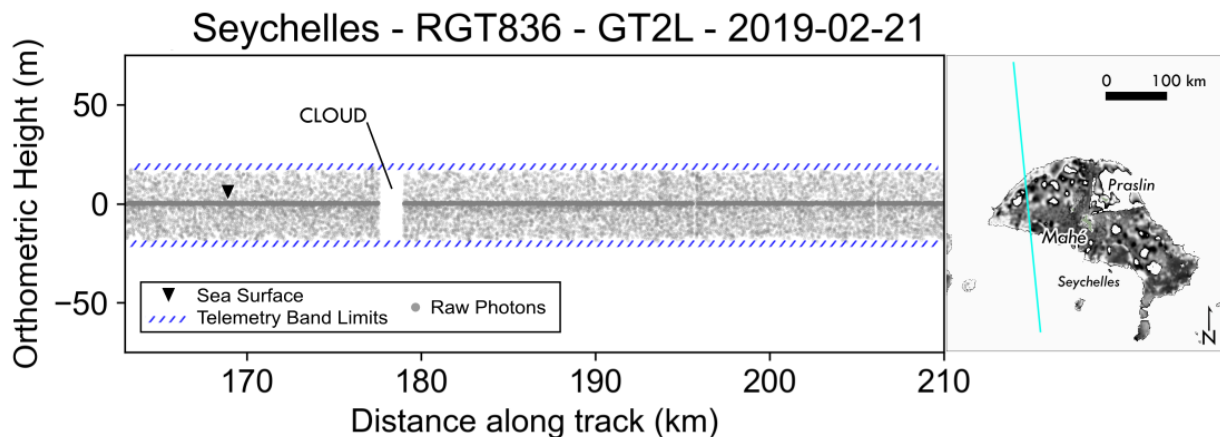
271  
 272 Figure 2. Due to the logic of handling the TEP within the receiver algorithms, some Major  
 273 Frames clip the ocean surface as it converges with the TEP. At about 80.75 seconds and 81.75  
 274 seconds the ocean surface is right at the bounds of the telemetry band, which is centered about  
 275 and sized for the TEP.  
 276

277 The second Knobs file update resolves an inconsistency between the receiver algorithms  
 278 and the flight software by removing the 140 m scale relief data (DRM-140) as an option for the  
 279 no-signal telemetry band relief in the timer2 state. The correct options for the no-signal telemetry  
 280 band relief in the timer2 state are the DEM (the nominal setting) or the 700 m scale relief data  
 281 (DRM-700). Note that both changes are replicated in the Alternate Knobs files where applicable.  
 282 The launch version of the PPR parameter files force the range windows for strong spots over sea  
 283 ice and land ice at night to a minimum of 5 km to capture the TEP. Because the TEP is only  
 284 present in two of the six spots (#1 and #3), the 5 km range window width minimum setting for  
 285 the remaining strong spot (#5) was reduced to the nominal minimum value of 500 meters.  
 286 At the request of the ICESat-2 Science Team, the telemetry band widths for the ocean, land ice  
 287 and sea ice surface types were increased in the ST files. The ocean telemetry bands gain 20  
 288 meters in total by increasing the telemetry band padding parameter by 10 meters, resulting in

289 ocean telemetry bands of 48 m in vertical height ( $\pm 24$  m above and below the signal). The land  
290 ice and sea ice telemetry bands are extended upwards by 30 meters to better capture blowing  
291 snow. This is accomplished by increasing the telemetry band padding by 15 meters and applying  
292 a -15-meter offset.

### 293 3.2 Version 10: Ocean Bathymetry

294 Several ICESat-2 Science Team members have focused on understanding the bathymetric  
295 capabilities of ATLAS once on-orbit and it was discovered that there were areas of clipped  
296 bathymetry data in open ocean tracks. This was due to the variable nature of the telemetry band  
297 limits along the coastlines and in open ocean. Figure 3 shows an example in the Indian Ocean in  
298 the Seychelles where shallow reef bathymetry has been excluded by the telemetry band size  
299 constraints. Bathymetric returns generally reach to 30 m below the water surface, and  
300 occasionally to 50 m (Parrish et al. 2019).



301  
302 Figure 3. An open ocean ground track showing the pre-Version 10 update telemetry band limits  
303 in the Seychelles. The shallow reef system to the west of Mahe island has known bathymetry that  
304 is less than 50 m deep and should be retrievable by ICESat-2, but has been excluded from the  
305 data because of the telemetry band limits (used with permission from Dietrich et al., 2023).  
306

307 Previously, the ocean telemetry bands spanned 48 m centered on the predicted surface,  
308 meaning they only reached 24 m below the surface. To reduce ocean bathymetry clipping, the

309 strong beam ocean telemetry bands were extended to reach at least 54 m below the surface by  
310 adjusting the padding and offset parameters. The vertical padding was increased by 15 m to 39 m  
311 and a vertical offset of +15 m is applied. The new padding and offset values extend the telemetry  
312 band deeper below the predicted surface while leaving the above surface limit unchanged.  
313 Utilizing the offset parameter allows for a smaller increase to the padding to extend to the  
314 desired depth, reducing the potential increase to the data volume. The padding and offset  
315 parameter changes are applied to the three strong spots and affect all ocean telemetry bands, not  
316 just areas with possible bathymetry (Dietrich et al. 2023).

317         Because the nominal parameters at the time of the version 10 update were set to not  
318 downlink weak spots data over oceans, no changes were made to the weak spot parameters  
319 because the weak spots are less likely to produce bathymetry (citations for less bathy in weak  
320 spots). A future (V13) update added the ability to telemeter weak spot ocean data., however the  
321 Version 10 changes for bathymetry capture are not applied as. The Alternate Knobs in version 10  
322 allowed for weak spot data to be downlinked, but the weak spot ocean telemetry bands did not  
323 have the increased padding and offset settings used in the strong spots. For more details on  
324 receiver algorithm updates related to bathymetric data acquisition (Versions 10 and 14), see  
325 Dietrich et al. (2023).

### 326         **3.3 Version 11: Range Window Error Mitigation**

327         In late 2020, an issue was discovered in which certain alignments of a strong/weak pair of  
328 range windows can trigger an error in the Data Flow Controller (DFC) logic, called a  
329 transmit/receive pulse (Tx/Rx) slip. When a Tx/Rx slip occurs, the ATL02 product generation  
330 code detects and corrects the error as detailed in Martino et al. ((Martino et al. 2019), Section  
331 2.5.7.3). In rare cases the error cannot be fixed with the current software, and the granule fails

332 before an ATL03 product file is generated. The error can be triggered at any time, but most  
333 frequently occurs when the range windows are forced “open”. In parameter file Versions 08  
334 through 10, the range windows for spots 1 and 3 are set to a minimum width of 5000 m to  
335 increase the frequency that the TEP can be captured. By forcing the range window for these  
336 strong spots to be much wider than they may be otherwise, the starts of the strong and weak spot  
337 range windows are more frequently farther apart, conditions which increase the likelihood of  
338 triggering the error. This is further supported by the decreased frequency of the error for PCE3,  
339 which does not include TEP, and whose strong-weak pair always have equivalent range window  
340 width minimums.

341 To mitigate the issue, the PPR files are updated to no longer force the range windows for  
342 spots 1 and 3 over land ice and sea ice at night to a minimum of 5000 m. The range window  
343 width minimums are updated to the nominal value of 500 m. This change does not fix the DFC  
344 logic error, but is a mitigation measure to decrease the frequency at which the error can occur.  
345 Additionally, the return to science mode sequence was updated on 27 May 2021 to further  
346 decrease the frequency of the error.

### 347 **3.4 Version 13: Ocean Weak Spots**

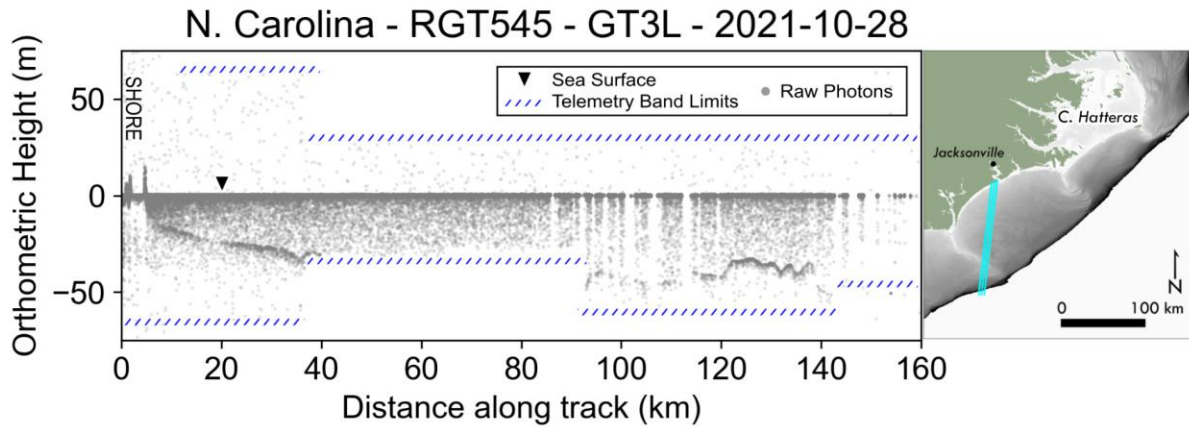
348 Prior to the Version 13 updates, weak spot ocean data was telemetered only when the  
349 Alternate Knobs were in use. Users of the Ocean Elevation Along-track Data Product (ATL12)  
350 found that weak spot returns have a sufficient signal-to-noise ratio to detect the ocean surface  
351 (Yu et al. 2021) and requested weak beam data to be consistently downlinked over the ocean.  
352 The utility of weak spot ocean data is further supported by the routine use in ICESat-2  
353 calibration scans which support spacecraft pointing and geolocation accuracy assessments  
354 (Luthcke et al. 2021). In the Knobs parameter files, the telemetry knobs for weak spot ocean

355 conditions were adjusted to downlink data when a Major Frame (nominally 200 pulses) or Super  
356 Frame (nominally 1000 pulses) signal is found. If no signal is found, then no data for weak spots  
357 is downlinked to minimize any increase in data volume. Note that the changes made in Version  
358 13 do not extend the telemetry bands for bathymetry that were introduced in Version 10 for the  
359 strong spots. Version 13 parameters became operational on 1 June 2021.

### 360 **3.5 Version 14: Coastline Bathymetry**

361 The increased ocean telemetry bands in Version 10 reduce bathymetry clipping in the  
362 open ocean, but that did not mitigate all of the instances of missing or clipped bathymetry data  
363 along coastlines. Figure 4 shows an example off the coast of North Carolina where the receiver  
364 algorithms set the telemetry band limits based on the land parameters, resulting in a loss of  
365 bathymetry. Because the on-board SRM can have multiple surface types in a single tile it  
366 prioritizes land over ocean when both are present in a SRM tile. As mentioned previously, the  
367 surface type dictates the level of vertical padding parameters for the telemetered data. Telemetry  
368 bands along coastlines therefore use the adjacent land parameters and, in some cases, lack the  
369 extended depth applied to the ocean telemetry bands because of the low relief values in the  
370 DRM.

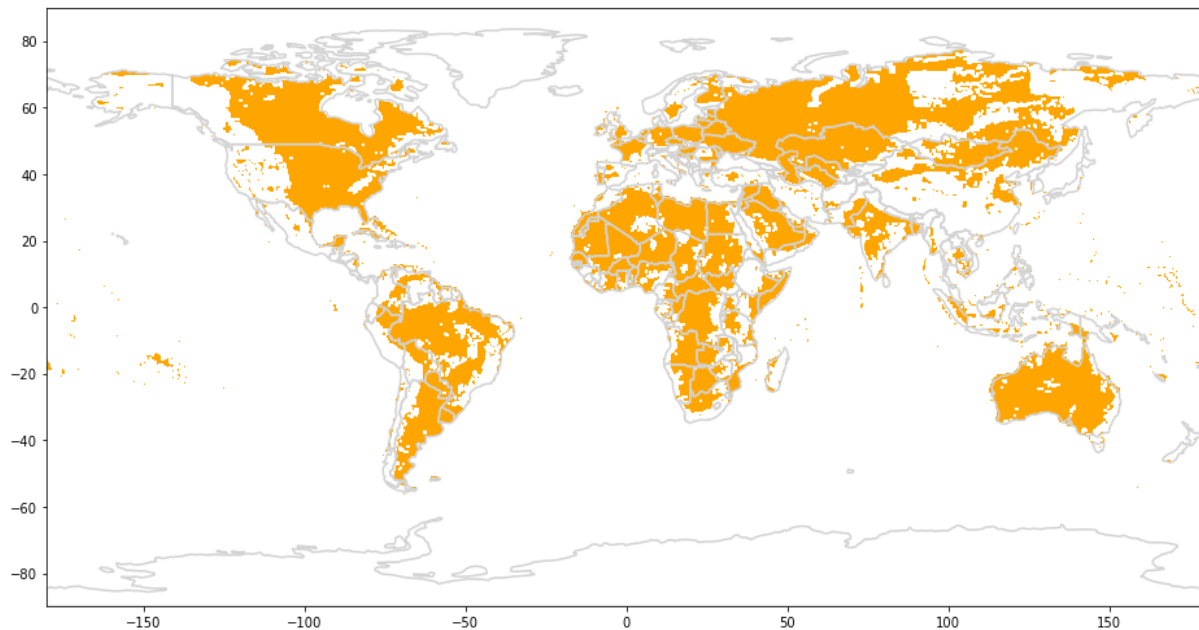
371



372  
 373 Figure 4. Bathymetric data loss after ocean telemetry band enhancements (v10) due to  
 374 prioritization of land in the on-board SRM, near the coast of North Carolina. Until 90 km along  
 375 track, the telemetry band parameters associated with land are in use when calculating the  
 376 telemetry band limits. (used with permission from Dietrich et al., 2023)  
 377

378 To correct the telemetry band settings in coastal areas two important considerations had  
 379 to be considered, the potential increases in data volume and reducing the likelihood of Did Not  
 380 Finish Major Frame (DNF MF) conditions (data transfer errors from the PCE cards). To create  
 381 the desired telemetry bands for coastal areas, the minimum padding over land for the strong spots  
 382 was increased by 30 m to approximately 54 m. This padding applies to all land areas with a  
 383 DRM relief value of 189 meters or less, highlighted in orange in Figure 5. The increase in the  
 384 minimum land padding reduces bathymetry clipping along coastlines where the SRM has not yet  
 385 switched from land to ocean. The changes are not applied to the weak spots, to remain consistent  
 386 with the previous ocean updates for capturing bathymetry (Version 10 and 13). These updates  
 387 became operational on-orbit on 1 December 2022. After this date, PCE1 and PCE3 each required  
 388 resetting. The resets result in gaps in Version 14 usage starting on 29 December 2022 for PCE1  
 389 and 2 February 2023 for PCE3. Version 14 became the permanent nominal parameters on all  
 390 PCEs on 6 February 2023.

391



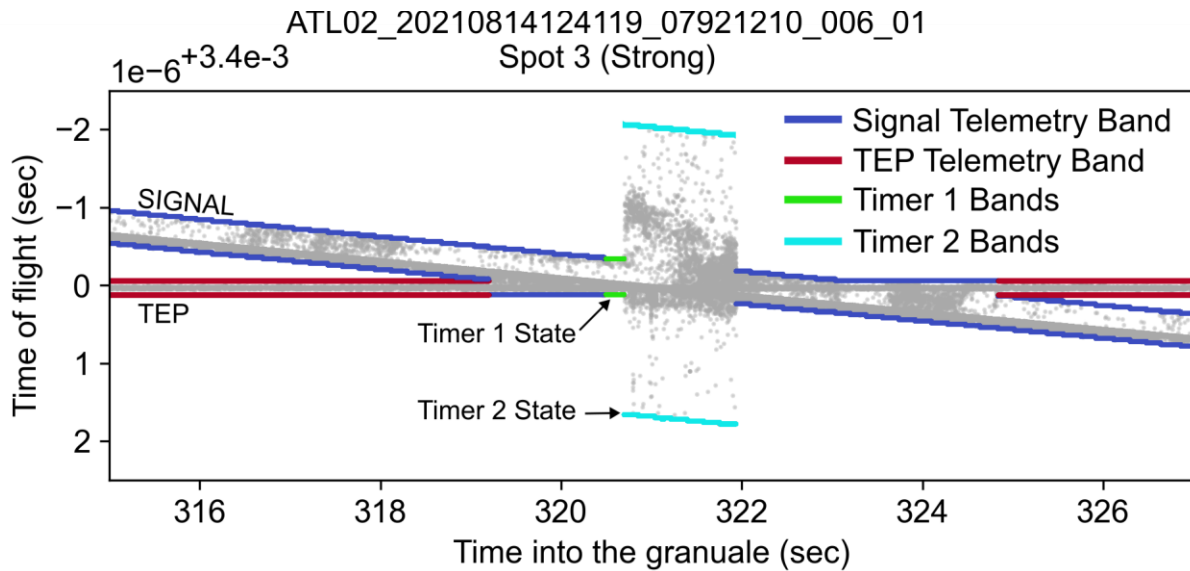
392  
393 Figure 5. Map of DRM tiles where the increased land padding is applicable. These tiles have a  
394 relief range of 0 to 189 meters.  
395

## 396 4. Results and Discussion

### 397 4.1 Version 08

398 Updates to the Knobs files in Version 08 mitigate the potential loss of data when the TEP  
399 crosses the ocean or sea ice surface due to the receiver algorithms' exclusion of the region about  
400 the TEP when searching for signal. When an ocean or sea ice surface enters the TEP region, the  
401 receiver algorithms enter the no-signal state and the updated Knobs are configured to continue  
402 telemetering the data using the no-signal state parameters. Figure 6 shows an example of the TEP  
403 crossing a sea ice surface. The Version 08 Knobs settings produce telemetry bands that  
404 successfully capture both the TEP and the surface as they intersect without any data clipping.  
405 When the surface enters the TEP region, the receiver algorithms first go into the no-signal timer1  
406 state and telemeter 10 Major Frames centered about the last known signal. After timer1  
407 concludes, the receiver algorithms switch to the no-signal timer2 state and telemeter bands that

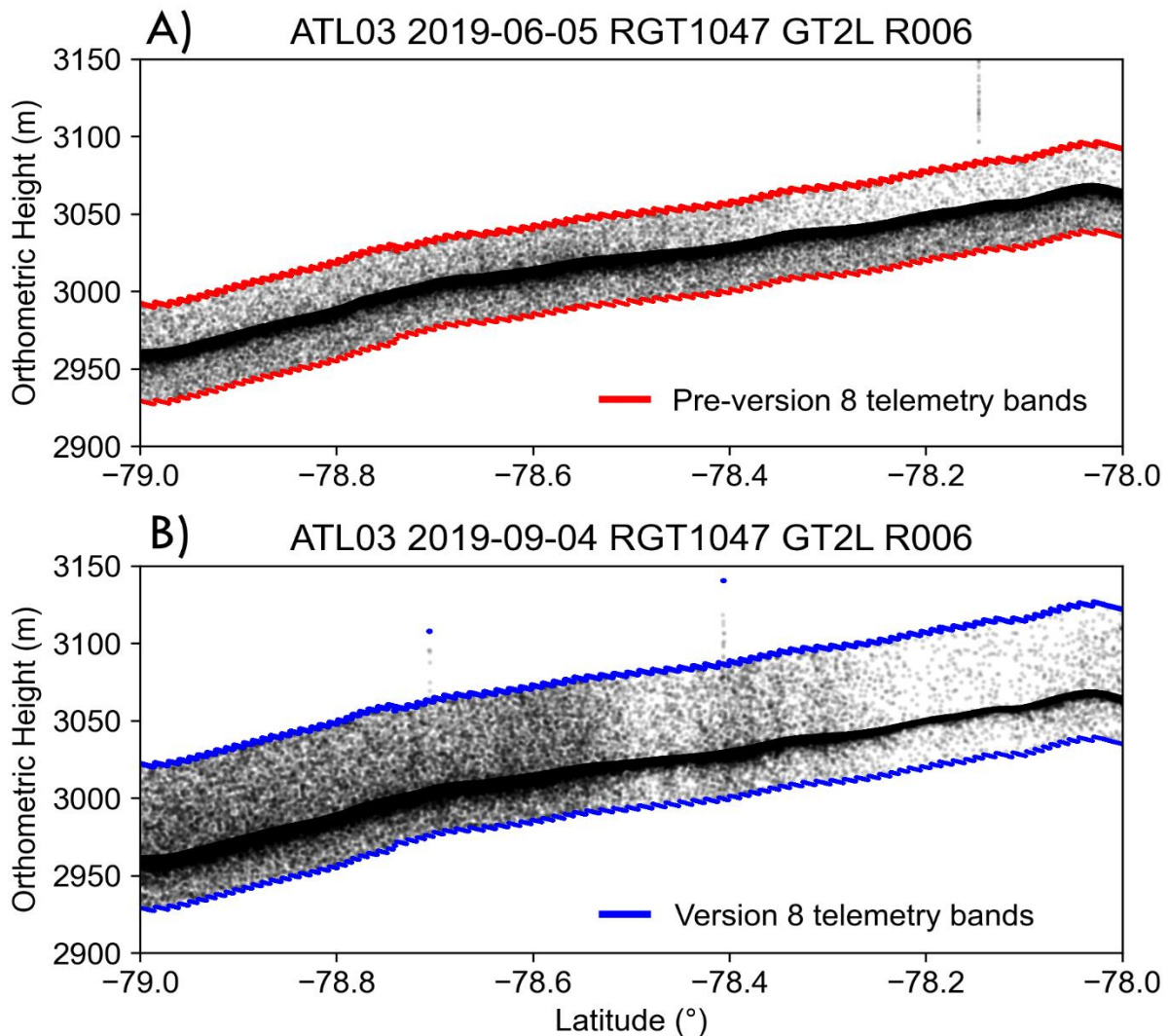
408 span the entire range window, ensuring surface is contained within the telemetry band. Timer2  
 409 concludes once a signal is found outside the TEP region. It is possible that both TEP and clouds,  
 410 or other noise features, are present in the range window. In such cases, noise features may be  
 411 selected as signal to be telemetered along with the TEP, and surface signals may be missed.  
 412



413  
 414 Figure 6. Example showing how the Version 8 changes for how the telemetry bands are  
 415 calculated for areas containing surface signal and TEP convergence.  
 416

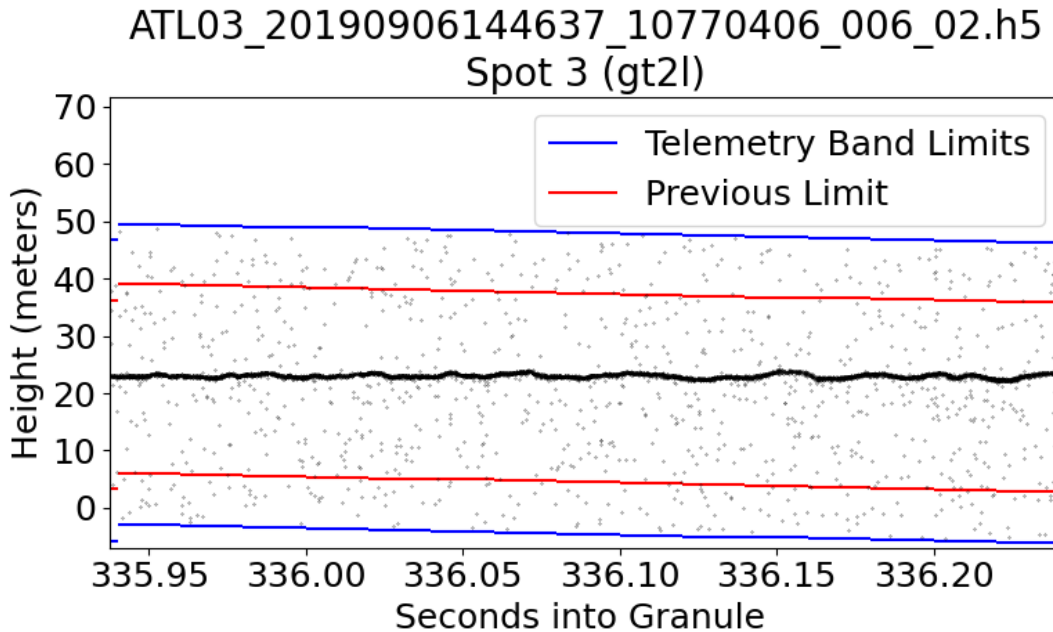
417 As the telemetry bands containing the surface signal (blue) and the telemetry bands containing  
 418 the TEP (red) converge, they first are combined into one telemetry band for each Major Frame  
 419 until the TEP is close enough to trigger the no-signal states, as shown in Figure 6. For ten Major  
 420 Frames the telemetry bands in the no-signal timer1 state (green) which are centered on the last  
 421 known signal location followed by over one second worth of the telemetry bands in the no-signal  
 422 timer2 state (cyan), which are centered within the range window. The telemetry bands go back to  
 423 a combined TEP and signal band once the signal is sufficiently out of the TEP region until they  
 424 are far enough apart to be telemetered separately.

425           The second update in Version 8 increased the telemetry band padding and offset  
426 parameter updates in the ST files for land ice and sea ice to increase the above surface portion of  
427 the telemetry band to better capture blowing snow. Blowing snow is an important component to  
428 understanding surface-atmosphere energy flux particularly in the polar regions (Herzfeld et al.  
429 2021) and this parameter change accommodates further investigations into these processes. All  
430 land ice and sea ice telemetry bands after the Version 08 update have an additional 30 meters in  
431 vertical width applied above the surface telemetry band limit, leaving the below surface limit  
432 unchanged, as described in Section 2. The total height above the surface in the telemetry band  
433 varies based on the relief value in the DRM. Figure 7 shows data from a portion of the same  
434 reference ground track in Antarctica (land ice) before and after Version 08 is made operational.  
435 The range in telemetry band widths increased by 30 meters, from 57 - 63 meters to 87 - 93  
436 meters. The surface is no longer centered in the telemetry band in Figure 7B since the additional  
437 30 meters of padding is expressed in the upper telemetry band limits.



438  
 439 Figure 7. Areas of blowing snow in Antarctica before (A) and after (B) the Version 08 updates  
 440 become operational. (A) On June 5, 2019, blowing snow is captured within the telemetry bands,  
 441 which have a vertical width ranging from approximately 57 to 63 meters. The surface signal is  
 442 centered within the telemetry bands, resulting in approximately 29.5 to 31.5 meters above the  
 443 surface available to capture blowing snow. (B) On September 4, 2019, additional blowing snow  
 444 is captured within the telemetry bands. The Version 08 updates produce telemetry bands with a  
 445 vertical width ranging from 87 to 93 meters with the additional 30 meters only applied to above  
 446 the surface. This results in approximately 59.5 to 61.5 meters of space above the surface to  
 447 capture blowing snow.  
 448

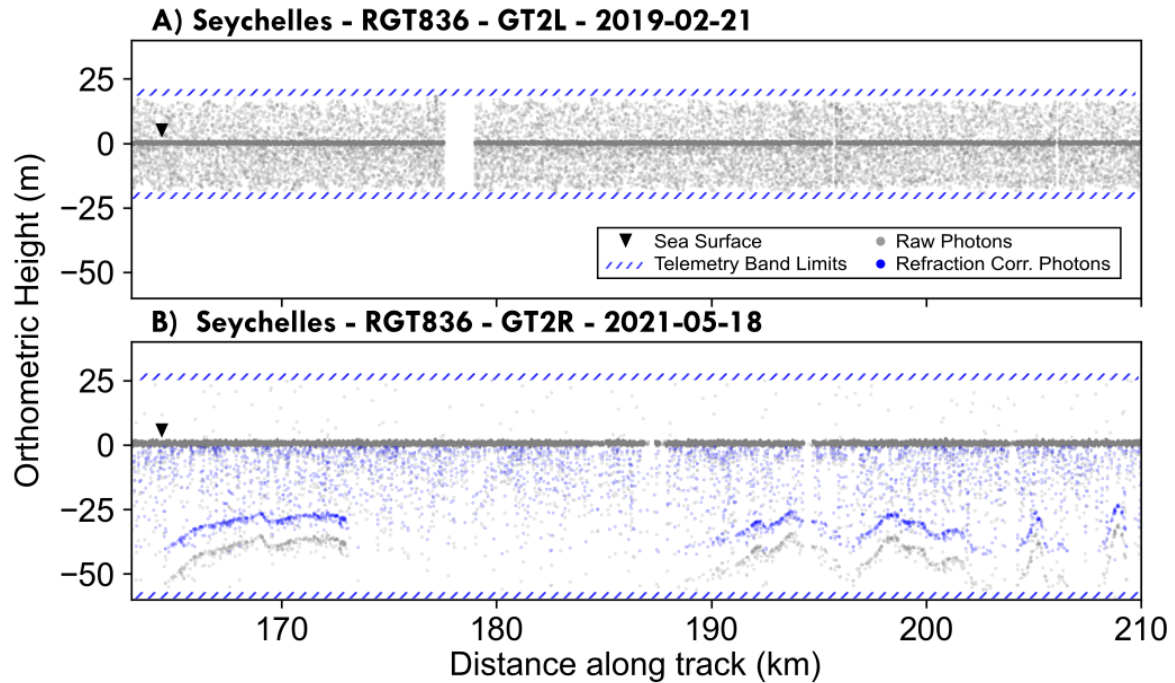
449 The third update implemented in Version 8 included small adjustments to telemetry  
 450 bands for the ocean surface type. The telemetry band padding parameter was increased to create  
 451 a total vertical band height of 48 m in vertical height ( $\pm 24$  m around the signal) (Figure 8).



452  
453 Figure 8. Telemetry over the ocean after the increase to the ocean telemetry band padding  
454 parameters. The Version 08 telemetry bands (blue) span a vertical width of ~51 meters, gaining  
455 ~10 meters both above and below the surface compared to the telemetry band limits prior to  
456 Version 08 (red).  
457

#### 458 **4.2 Version 10**

459 By extending the strong spot telemetry bands over ocean to 54 meters below the surface,  
460 bathymetry previously excluded in the data can now be captured. More specifically, potential  
461 bathymetry that falls below the previous telemetry band lower limit of 24 meters below the  
462 surface to the updated lower limit of 54 meters is now included in the downlinked data. Figure 9  
463 shows an example near the Seychelles where potential bathymetry is captured in the extended  
464 portion of the telemetry band. See Dietrich et al. (Dietrich et al. 2023) for additional details and  
465 examples.



466 Figure 9. Telemetry bands for reference ground track (RGT) 0836 in the Seychelles. a) illustrates  
 467 the telemetry bands before the Version 10 update showing no bathymetry. b) highlights the  
 468 expanded telemetry bands of Version 10 and the newly available reef bathymetry that was  
 469 previously not recorded (used with permission from Dietrich et al., 2023).  
 470  
 471

### 472 4.3 Version 11

473 The range window settings in Version 08 introduced, at times, large differences in the  
 474 range window starts of strong-weak pairs for PCEs 1 and 2. These differences are often on the  
 475 order of 2 kilometers or more. As described above, this condition increases the likelihood of  
 476 Tx/Rx slips. The range window adjustments in Version 11 reduce the differences in range  
 477 window starts to an average of a few meters or less, consistent with measurements for PCE 3.

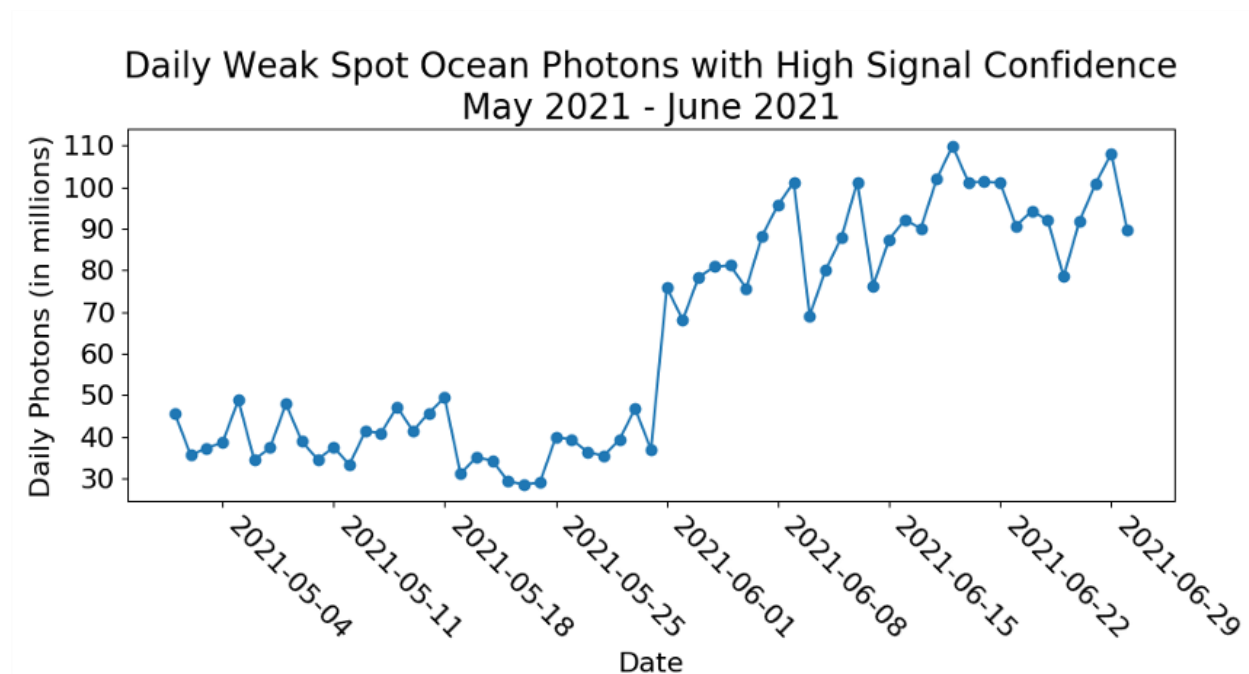
478 The Version 11 mitigation successfully reduced the conditions favorable for TxRx slips  
 479 introduced in Version 08. In Versions 08 through 10, TxRx slips occurred in 1,759 granules, or  
 480 1.54% of data over ~1.5 years. After the Version 11 update, TxRx slips occurred in just 314  
 481 granules, or 0.15% of data over more than 2.5 years as of this writing. Note that these figures  
 482 consider only the most common TxRx slip type, corrected in ATL02 (A. Martino, Field, and

483 Ramos-Izquierdo 2020).

#### 484 **4.4 Version 13**

485 Version 13 became operational on June 1, 2021, greatly increasing the amount of weak  
486 spot data available over the open oceans. Figure 10 shows the daily number of weak spot, ocean  
487 photons with high signal confidence in ATL03 (Neumann et al. 2019) for 1 May and 31 June  
488 2021, with a distinct jump on June 1, 2021 when Version 13 became operational. The ATL03  
489 weak spot, ocean data for May 2021 were data that were collected when the Alternate Knobs are  
490 in use (17 ocean scans, 8 round-the-world scans, and parts of the 42 ocean targets of opportunity  
491 (TOOs)) and times when the on-board SRM classification of ocean does not align with the  
492 ATL03 surface type classification. Because June 2021 has only one additional ocean scan and  
493 round-the-world scan, the increase in high signal confidence weak spot, ocean data can be  
494 attributed to the Version 13 parameter update. The addition of weak spot, ocean telemetry  
495 increases its fraction of the total data telemetered by approximately 1%. This small increase in  
496 percentage of data telemetered is expected due to the small size of the telemetry band (48 meters)  
497 and the reduced photon rate for weak-spots.

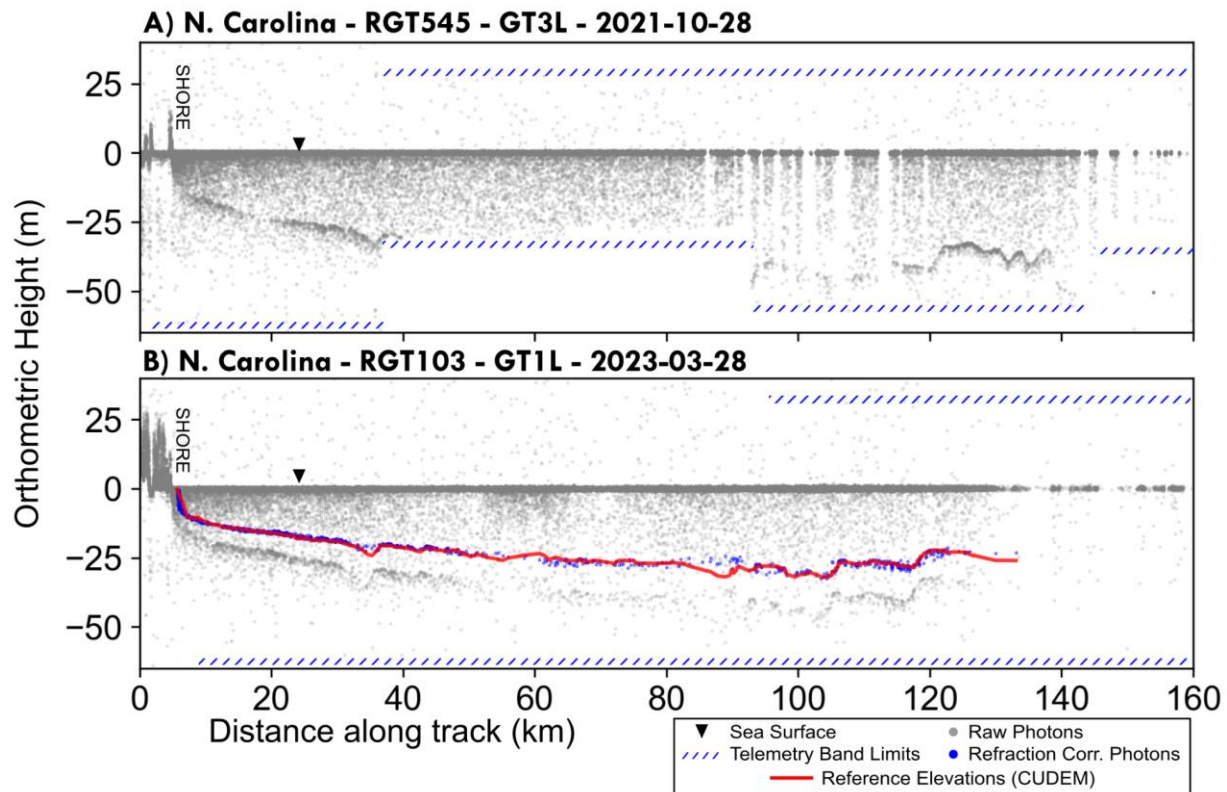
498 A recent example of the utility of using the weak beam data is the recovery of ocean  
499 wave characteristics, particularly nearshore where the dynamics are more complex.  
500 Understanding wave direction and the overall geometry of wave motion is only possible with the  
501 correlation of signal between two beams, in this case a pair (Dietrich, Magruder, and Holwill  
502 2023). It is anticipated that the inclusion of the weak spot will foster more science discovery  
503 moving forward as the mission accumulates data in relevant locations and extends coverage.



504  
 505 Figure 10. Daily sum of high signal weak spot, ocean photons in ATL03 from 05/01/2021 to  
 506 06/30/2021. The step increase in weak spot, ocean signal photons apparent on 06/01/2021 is due  
 507 to the Version 13 update becoming operational.  
 508

#### 509 **4.5 Version 14**

510 The majority of the bathymetry potentially observable by ICESat-2 falls along coastlines  
 511 where the receiver algorithms set the telemetry band limits based on the parameters  
 512 corresponding to land surface type. The Version 10 updates include only parameters  
 513 corresponding to ocean surface type, so a large portion of potential bathymetry was not captured  
 514 by those updates. The Version 14 updates extend the land telemetry bands to at least as deep as  
 515 the ocean bands for areas that have a relief value less than or equal to 189 meters from the DRM.  
 516 Figure 11b shows the effect of the version 14 updates compared to the previous band limits  
 517 (Figure 11a and Figure 4). See Dietrich et al. (Dietrich et al. 2023) for a detailed study on how  
 518 much additional potential bathymetry the Version 14 and Version 10 updates provide.



519  
 520 Figure 11. Newly available bathymetry off the coast of North Carolina, USA after the Version 14  
 521 update. a) Previous telemetry band limits highlighting the clipped bathymetry caused by the  
 522 switching from land to ocean surface parameters and b) newly available continuous bathymetric  
 523 profile made possible by the consistent lower telemetry band limit of -54 meters below the  
 524 surface. Refraction corrected photon elevations are shown in blue with a comparison to NOAA  
 525 CUDEM elevations. (used with permission from Dietrich et al., 2023)  
 526

## 527 6. Conclusions

528 The ICESat-2/ATLAS receiver algorithms have had several updates since the launch of  
 529 the satellite in 2018. These modifications were motivated by a desire to optimize (further) the  
 530 science that the ICESat-2 measurements are able to facilitate and also to mitigate some  
 531 operational issues. This paper is a result of many scientists and engineers evaluating the icesat-2  
 532 data and highlights the exceptional response of the ICESat-2 project office to providing the  
 533 scientific community the quality of data that meets multi-disciplinary standards despite not being  
 534 part of the prime mission objectives. It is expected that these new adjustments and

535 accommodations will allow for enhanced research and discovery in many areas of Earth science.  
536 The software changes onboard were possible because of the careful planning and insight of the  
537 ATLAS engineers to enable adjustments to the quantity and quality of signals collected. ICESat-  
538 2 is an example of adaptability and resilience on-orbit to ensure that the mission is optimized for  
539 data collection that maximizes the scientific return.

#### 540 **Acknowledgments**

541 The authors wish to thank the ICESat-2 Project Science Office for the support as well as  
542 the NASA HQ support under grant #80NSSC23K0044. We also thank Alvaro Ivanoff for the  
543 data volume statistics around the Version 13 update and related figure.

#### 544 **Data Availability**

545 All data used in this publication is publicly available from the National Snow and Ice  
546 Data Center (<https://nsidc.org/>) from ATL02 and ATL03 ICESat-2 data products.

#### 547 **References**

- 548 Dietrich, James, Lori Magruder, and Matthew Holwill. 2023. "Monitoring Coastal Waves with  
549 ICESat-2." *Journal of Marine Science and Engineering* In pre-print. [https://doi.org/Doi:  
550 10.20944/preprints202310.1185.v1](https://doi.org/Doi:10.20944/preprints202310.1185.v1).
- 551 Dietrich, James, Ann R Rackley Reese, Aimée Gibbons, Lori A. Magruder, and Christopher  
552 Parrish. 2023. "Analysis of ICESat-2 Data Acquisition Algorithm Parameter  
553 Enhancements to Improve Worldwide Bathymetric Coverage." Preprint. Preprints.  
554 <https://doi.org/10.22541/essoar.169447414.45310708/v1>.
- 555 Herzfeld, Ute, Adam Hayes, Stephen Palm, David Hancock, Mark Vaughan, and Kristine  
556 Barbieri. 2021. "Detection and Height Measurement of Tenuous Clouds and Blowing  
557 Snow in ICESat-2 ATLAS Data." *Geophysical Research Letters* 48 (17).  
558 <https://doi.org/10.1029/2021GL093473>.
- 559 Jarvis, A., Hannes Reuter, Andy Nelson, and Edith Guevara. 2008. "Hole-Filled SRTM for the  
560 Globe Version 3, from the CGIAR-CSI SRTM 90m Database." *See Http://Srtm. Csi.*  
561 *Cgiar. Org*, January.
- 562 Leigh, Holly W., Lori A. Magruder, Claudia C. Carabajal, Jack L. Saba, and Jan F. McGarry.  
563 2015. "Development of Onboard Digital Elevation and Relief Databases for ICESat-2."  
564 *IEEE Transactions on Geoscience and Remote Sensing* 53 (4): 2011–20.  
565 <https://doi.org/10.1109/TGRS.2014.2352277>.
- 566 Luthcke, S. B., T. C. Thomas, T. A. Pennington, T. W. Rebold, J. B. Nicholas, D. D. Rowlands,  
567 A. S. Gardner, and S. Bae. 2021. "ICESat-2 Pointing Calibration and Geolocation

- 568 Performance.” *Earth and Space Science* 8 (3). <https://doi.org/10.1029/2020EA001494>.
- 569 Magruder, Lori, Kelly Brunt, Thomas Neumann, Bradley Klotz, and Michael Alonzo. 2021.
- 570 “Passive Ground-Based Optical Techniques for Monitoring the On-Orbit ICESat-2
- 571 Altimeter Geolocation and Footprint Diameter.” *Earth and Space Science* 8 (10).
- 572 <https://doi.org/10.1029/2020EA001414>.
- 573 Magruder, Lori, Thomas Neumann, and Nathan Kurtz. 2021. “ICESat-2 Early Mission Synopsis
- 574 and Observatory Performance.” *Earth and Space Science* 8 (5).
- 575 <https://doi.org/10.1029/2020EA001555>.
- 576 Magruder, Lori, Tom Neumann, Nathan Kurtz, and Tyler Sutterley. 2024. “The Ice, Cloud and
- 577 Land Elevation Satellite-2: Meeting the Prime Mission Science Requirements.” *Remote*
- 578 *Sensing of Environment*, no. In review.
- 579 Markus, Thorsten, Tom Neumann, Anthony Martino, Waleed Abdalati, Kelly Brunt, Beata
- 580 Csatho, Sinead Farrell, et al. 2017. “The Ice, Cloud, and Land Elevation Satellite-2
- 581 (ICESat-2): Science Requirements, Concept, and Implementation.” *Remote Sensing of*
- 582 *Environment* 190 (March): 260–73. <https://doi.org/10.1016/j.rse.2016.12.029>.
- 583 Martino, A. J., M. R. Bock, R. L. Jones III, T. A. Neumann, D. Hancock, P. W. Dabney, and C.
- 584 E. Webb. 2019. “ATLAS/ICESat-2 L1B Converted Telemetry Data, Version 1.” NASA
- 585 National Snow and Ice Data Center Distributed Active Archive Center.
- 586 <https://doi.org/10.5067/ATLAS/ATL02.001>.
- 587 Martino, Anthony, Christopher T Field, and Luis Ramos-Izquierdo. 2020. “ICESat-2/ATLAS
- 588 Instrument Linear System Impulse Response.” Preprint. Geophysics.
- 589 <https://doi.org/10.1002/essoar.10504651.1>.
- 590 Martino, Anthony J., Thomas A. Neumann, Nathan T. Kurtz, and Douglas McLennan. 2019.
- 591 “ICESat-2 Mission Overview and Early Performance.” In *Sensors, Systems, and Next-*
- 592 *Generation Satellites XXIII*, 11151:68–77. SPIE. <https://doi.org/10.1117/12.2534938>.
- 593 McGarry, J. F., C. C. Carabajal, J. L. Saba, A. R. Reese, S. T. Holland, S. P. Palm, J.-P. A.
- 594 Swinski, J. E. Golder, and P. M. Liiva. 2021. “ICESat-2/ATLAS Onboard Flight Science
- 595 Receiver Algorithms: Purpose, Process, and Performance.” *Earth and Space Science* 8
- 596 (4). <https://doi.org/10.1029/2020EA001235>.
- 597 Neumann, Thomas A., Anthony J. Martino, Thorsten Markus, Sungkoo Bae, Megan R. Bock,
- 598 Anita C. Brenner, Kelly M. Brunt, et al. 2019. “The Ice, Cloud, and Land Elevation
- 599 Satellite – 2 Mission: A Global Geolocated Photon Product Derived from the Advanced
- 600 Topographic Laser Altimeter System.” *Remote Sensing of Environment* 233 (November):
- 601 111325. <https://doi.org/10.1016/j.rse.2019.111325>.
- 602 Parrish, Christopher E., Lori A. Magruder, Amy L. Neuenschwander, Nicholas Forfinski-
- 603 Sarkozi, Michael Alonzo, and Michael Jasinski. 2019. “Validation of ICESat-2 ATLAS
- 604 Bathymetry and Analysis of ATLAS’s Bathymetric Mapping Performance.” *Remote*
- 605 *Sensing* 11 (14): 1634. <https://doi.org/10.3390/rs11141634>.
- 606 Schutz, B. E., H. J. Zwally, C. A. Shuman, D. Hancock, and J. P. DiMarzio. 2005. “Overview of
- 607 the ICESat Mission.” *Geophysical Research Letters* 32 (21): L21S01.
- 608 <https://doi.org/10.1029/2005GL024009>.
- 609 Simard, Marc, Naiara Pinto, Joshua B. Fisher, and Alessandro Baccini. 2011. “Mapping Forest
- 610 Canopy Height Globally with Spaceborne Lidar.” *Journal of Geophysical Research* 116
- 611 (G4): G04021. <https://doi.org/10.1029/2011JG001708>.
- 612 Smith, Ben, Helen A. Fricker, Alex S. Gardner, Brooke Medley, Johan Nilsson, Fernando S.
- 613 Paolo, Nicholas Holschuh, et al. 2020. “Pervasive Ice Sheet Mass Loss Reflects

614           Competing Ocean and Atmosphere Processes.” *Science* 368 (6496): 1239–42.  
615           <https://doi.org/10.1126/science.aaz5845>.  
616 Yu, Yao, David T Sandwell, Sarah T Gille, and Ana Beatriz Villas Bôas. 2021. “Assessment of  
617 ICESat-2 for the Recovery of Ocean Topography.” *Geophysical Journal International*  
618 226 (1): 456–67. <https://doi.org/10.1093/gji/ggab084>.  
619